NASA/TM—2010-216961

Atmospheric Turbulence Modeling for Aero Vehicles: Fractional Order Fits

George Kopasakis
Glenn Research Center, Cleveland, Ohio

December 2010

NASA STI Program . . . in Profile

Since its founding, NASA has been dedicated to the advancement of aeronautics and space science. The NASA Scientific and Technical Information (STI) program plays a key part in helping NASA maintain this important role.

The NASA STI Program operates under the auspices of the Agency Chief Information Officer. It collects, organizes, provides for archiving, and disseminates NASA's STI. The NASA STI program provides access to the NASA Aeronautics and Space Database and its public interface, the NASA Technical Reports Server, thus providing one of the largest collections of aeronautical and space science STI in the world. Results are published in both non-NASA channels and by NASA in the NASA STI Report Series, which includes the following report types:

- TECHNICAL PUBLICATION. Reports of completed research or a major significant phase of research that present the results of NASA programs and include extensive data or theoretical analysis. Includes compilations of significant scientific and technical data and information deemed to be of continuing reference value. NASA counterpart of peer-reviewed formal professional papers but has less stringent limitations on manuscript length and extent of graphic presentations.

- TECHNICAL MEMORANDUM. Scientific and technical findings that are preliminary or of specialized interest, e.g., quick release reports, working papers, and bibliographies that contain minimal annotation. Does not contain extensive analysis.

- CONTRACTOR REPORT. Scientific and technical findings by NASA-sponsored contractors and grantees.

- CONFERENCE PUBLICATION. Collected papers from scientific and technical conferences, symposia, seminars, or other meetings sponsored or cosponsored by NASA.

- SPECIAL PUBLICATION. Scientific, technical, or historical information from NASA programs, projects, and missions, often concerned with subjects having substantial public interest.

- TECHNICAL TRANSLATION. English-language translations of foreign scientific and technical material pertinent to NASA's mission.

Specialized services also include creating custom thesauri, building customized databases, organizing and publishing research results.

For more information about the NASA STI program, see the following:

- Access the NASA STI program home page at *http://www.sti.nasa.gov*

- E-mail your question via the Internet to *help@sti.nasa.gov*

- Fax your question to the NASA STI Help Desk at 443–757–5803

- Telephone the NASA STI Help Desk at 443–757–5802

- Write to:
  NASA Center for AeroSpace Information (CASI)
  7115 Standard Drive
  Hanover, MD 21076–1320

NASA/TM—2010-216961

Atmospheric Turbulence Modeling for Aero Vehicles: Fractional Order Fits

George Kopasakis
Glenn Research Center, Cleveland, Ohio

National Aeronautics and
Space Administration

Glenn Research Center
Cleveland, Ohio 44135

December 2010

Acknowledgments

The author would like to acknowledge the support of the NASA Supersonics Project for the research conducted in this paper.

This work was sponsored by the Fundamental Aeronautics Program
at the NASA Glenn Research Center.

Level of Review: This material has been technically reviewed by technical management.

Available from

NASA Center for Aerospace Information
7115 Standard Drive
Hanover, MD 21076–1320

National Technical Information Service
5301 Shawnee Road
Alexandria, VA 22312

Available electronically at http://gltrs.grc.nasa.gov

Atmospheric Turbulence Modeling for Aero Vehicles: Fractional Order Fits

George Kopasakis
National Aeronautics and Space Administration
Glenn Research Center
Cleveland, Ohio 44135

Abstract

Atmospheric turbulence models are necessary for the design of both inlet/engine and flight controls, as well as for studying coupling between the propulsion and the vehicle structural dynamics for supersonic vehicles. Models based on the Kolmogorov spectrum have been previously utilized to model atmospheric turbulence. In this paper, a more accurate model is developed in its representative fractional order form, typical of atmospheric disturbances. This is accomplished by first scaling the Kolmogorov spectral to convert them into finite energy von Karman forms and then by deriving an explicit fractional circuit-filter type analog for this model. This circuit model is utilized to develop a generalized formulation in frequency domain to approximate the fractional order with the products of first order transfer functions, which enables accurate time domain simulations. The objective of this work is as follows. Given the parameters describing the conditions of atmospheric disturbances, and utilizing the derived formulations, directly compute the transfer function poles and zeros describing these disturbances for acoustic velocity, temperature, pressure, and density. Time domain simulations of representative atmospheric turbulence can then be developed by utilizing these computed transfer functions together with the disturbance frequencies of interest.

Introduction

This paper addresses the need for a model that simulates atmospheric disturbance, in both the time and frequency domain, over a wide range of altitudes and variations in atmospheric turbulence conditions, that is relatively easy to implement and representative of the actual fractional order nature of atmospheric turbulence. This is applicable to both propulsion system flow field type disturbances as well as vehicle gust loads.

Atmospheric turbulence have been studied for some time, especially in the field of Atmospheric Sciences, Nastrom (1985), and Fairall (1991), and various models have been developed. These models are primarily based on the so called Kolmogorov spectrum, originally developed by Tatarski (1961), based partly on the studies of turbulence by the Russian mathematician Andrei Kolmogorov (Kolmogorov (1941) (a) and (b)). The Kolmogorov spectrum has an energy level that approaches infinity as frequency approaches zero. This characteristic makes it difficult to implement these types of models in the time domain. A suitable approximation to the Kolmogorov model that is commonly used with a finite energy spectrum is the von Karman type model, originally referred to as the isotropic-turbulence spectrum, (Houbolt (1964)). However, simulating the von Karman type models in the time domain is still problematic because of their fractional order. The Kolmogorov model has also been extended (Tank (1994)) to develop a baseline of atmospheric turbulence for the High Speed Civil Transport (HSCT). The Tank model also covers atmospheric acoustic wave disturbance modeling utilizing the von Karman spectral. Hoblit (1988) introduced the Dryden model approximation to the fractional order von Karman atmospheric model. But this model is second order compared to the 5/3 fractional order of the acoustic velocity atmospheric turbulence spectral. Thus, the Dryden model underestimates the atmospheric disturbances, increasingly with frequency.

To alleviate some of these difficulties, the Tank model for the von Karman approximation is utilized in this paper to derive an explicit electrical circuit analog of atmospheric disturbances. This circuit analog will act as a low pass filter. The circuit elements are explicitly computed as functions of atmospheric parameters, such as eddy dissipation rate and integral length scale. However, like the actual atmospheric disturbances, Nastrom (1985), the circuit order also turns out to be fractional order, which makes it difficult to simulate. Thus, the circuit model is used as the basis in this development to derive integer order transfer function (TF) approximations to the fractional order model. These TF approximations are a product of first order poles and zeros, which are determined as a function of the parameters describing an atmospheric disturbance. This approach alleviates the manual process of hand fitting the approximation every time an atmospheric parameter is changed.

Fairall (1991), Tank ((1994) and (1996)) and others approach atmospheric disturbance modeling probabilistically, as an *exceedance* for controls design purposes. That means that the probability of a time to failure is computed for controls design. This time to failure is associated with a controls design that can tolerate a maximum specified disturbance, and computes the probability, in terms of flight miles or hours, that an atmospheric disturbance will exceed this threshold. In this paper the approach will be to compute the worst case disturbance expected, and assume that the control system will be designed to handle this disturbance. Thus, this paper will not cover *exceedance rates*, which can be computed separately, based on the worst disturbance expected and the specifics of the controls design.

Kopasakis (2010) extends the work discussed in this paper to cover considerations for atmospheric turbulence specifications for supersonic propulsion systems. This work also provides an example for a supersonic inlet shock position controls design in the presence of atmospheric turbulence.

This paper is organized as follows. First, the Kolmogorov form of the atmospheric disturbance spectrum is presented followed by the Tank model for the von Karman spectrum forms of the acoustic disturbances. This is followed with formulations of the equivalent fractional order TF approximations of atmospheric turbulence. Finally, time domain atmospheric disturbances are discussed for the derived TF approximations, followed by concluding remarks. The formulations covered in the body of the paper are based on an electrical circuit analog developed for different types of atmospheric disturbances, which is covered in Appendix B. While the detailed derivations of these formulations are covered in Appendix C.

Kolmogorov Form of the Atmospheric Disturbance Model

Tank ((1994) and (1996)) utilizes a Kolmogorov one-dimensional locally isotropic atmospheric turbulence spectrum, mathematically developed in Tatarski (1961), which represents the spectral density of a structured random field of atmospheric turbulence as

$$S_t(k) = \alpha_t \varepsilon^{2/3} k^{-5/3} \tag{1}$$

In this equation the quantity ε signifies the eddy dissipation rate, in units of (energy/(mass × time)) = (m^2/sec^3), and k signifies the wavenumber, in units of (rad/m) or (cycles/m). The subscript t in the atmospheric turbulence spectral density, $S_t(k)$, signifies the type of disturbance. Based on these definitions, the units of $S_t(k)$ are $(m/sec)^2/(rad/m)$ (Tatarski (1961)), where the units of rad or Hz are not affected by raising them to a power. Or $S_t(k)$ *will have* units of $(m/sec)^2/(cycle/m)$ (Tank (1994)), as rad = cycle/2π, with the 2π factor that multiplies the spectral density for this conversion absorbed into the constants α_t terms. In this treatment, more convenient units in terms of Hz will be utilized as $((m/sec)^3/Hz)$, by substituting cycles with Hz*sec, which allows displaying results in terms of the acoustic wave velocity in (m/sec) /Hz.

Tatarski (1961) includes a more detailed treatment of ε along with a detailed derivation of Equation (1). In brief, $\varepsilon = \nu * v_l'^2 / l^2$ is called the eddy dissipation rate and it represents the energy dissipated as heat per unit mass per unit time due to a velocity fluctuation that occurs in an atmospheric region of size (length) l, due to a flow instability that takes place when a certain critical Reynolds number value is exceeded (Tatarski (1961)). This critical Reynolds number cannot be determined precisely, but for worst case atmospheric turbulence calculations it would be correct to assume that this number is exceeded. The quantity ν is the kinematic viscosity, and v_l' is a velocity fluctuation in an atmospheric region of size l.

At lower altitudes, the eddy dissipation rate can vary significantly with altitude and severity of turbulence (Fairall (1991)) as well as globally (Nastrom (1985)). Tank (1994) used a worst value of 8.6e–5 based on data collected at altitudes ranging from 25,000 to 40,000 ft (~ 7.5 to 12 km), which is about four times the appropriate value of ε for North Atlantic cruise altitudes. For supersonic cruise altitude, around 60,000 ft (~18 km), the same value of ε can be used, as ε is relatively constant at altitudes above 20,000 ft (~6 km).

According to Tatarski (1961), Equation (1) holds for turbulence lengths much greater than what would be considered a microstructure (10's of meters) for eddy dissipation and much less than the long length scale (that is considered to be about 400 km). Some sparse measurements performed by Obukhov (1949) in the lower troposphere agree with Equation (1), as well as other measurements by Nastrom (1985). The constant α_t is constant for each type of disturbance, given by Tank 1994, to fit observed data:

$\alpha_l = 0.15$	(longitudinal wind velocity gust, dimensionless)
$\alpha_v = 0.2$	(vertical or horizontal wind velocity gust, dimensionless)
$\alpha_T = 0.39$	(temperature disturbance, $K^2s^2m^{-2}$)
$\alpha_P = 0.0005(P_o/T_o)^2$	(pressure disturbance, $Pa^2s^2m^{-2}$), where the subscript "o" denotes total atmospheric quantities.

For a flight vehicle encountering an atmospheric disturbance, the disturbance frequency is defined as

$$f = \frac{Ma}{\lambda} = kMa \tag{2}$$

Where M is the vehicle Mach number, a is the local speed of sound (m/sec), λ is the wave length of the atmospheric disturbance (m/cycle), and k is 1/λ (cycles/m). The disturbance frequency is based on an aero vehicle traveling at a certain altitude and Mach number that encounters an atmospheric disturbance with a certain wavelength. There would be a corresponding frequency based on Equation (2) around which atmospheric disturbances will be exhibited. However, a control design would need to be able to sufficiently attenuate these disturbances under a wide range of flight and atmospheric conditions. Thus, accounting for the full operating envelope, a controls design would need to attenuate atmospheric disturbances in a wide range of frequencies. Normally, lower frequency atmospheric disturbances will be easier for the control design to handle.

The speed of sound is related with temperature as

$$a = \sqrt{\gamma R T_s} \tag{3}$$

where T_s is the static temperature in K.

According to the International Standard Atmosphere (ISA) or (Anderson (2000)), the temperature decreases at a rate of approximately 6.5 K per km, from sea level up to 36,000 ft (~11 km). From 36,000 to 65,000 ft (~11 to 20 km) which would be the approximate cruise altitude of a supersonic transport, the temperature remains constant at about 216 K. Thus, temperature (K) as a function of altitude, h (km), can be expressed as

$$T(h) = T_{oh} - 6.5(h - h_{oh}) \tag{4}$$

where T_{oh} is the temperature at an arbitrary reference height h_{oh}, which is accurate up to 36,000 ft and then stays constant above that. Based on that, at supersonic cruise conditions the speed of sound would be approximately 295 m/sec.

Figure 1 shows the zonal (east-west) winds, meridional (north-south) wind, and potential temperature power spectral as reported in Nastrom (1985). The units of the wind power spectral are in (m^3/sec^2)/rad and temperature is in (K^2m/rad). As shown in this figure, at the long length scale (i.e., beyond 400 km) the power of turbulence decreases as the –3 power with decreasing wavelength (increasing frequency), thereafter decreasing as the –5/3 power which agrees with Equation (1). Therefore, Equation (1) shows a good representation of the atmospheric spectral density with a wavelength smaller than 400 km.

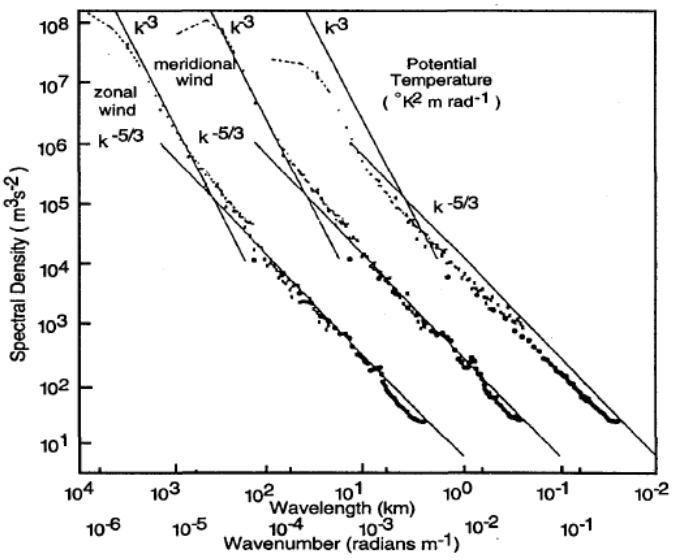

Figure 1.—Wind and Potential Temperature Spectra as reported by Nastrom (1985). Note: for clarity, the meridional wind and potential temperature spectra have been shifted one and two decades to the right, respectively.

The Tank Model of the Atmospheric Disturbance

As an alternative to the Kolmogorov spectrum, Tank (Soreide and Tank (1996) and (1997)) scaled the von Karman spectrum to fit the Kolmogorov model in the limit (i.e., for large k), which compares well with other data. For longitudinal disturbances this spectrum is

$$S_{l,VK}(k) = 2.7\varepsilon^{2/3}L^{5/3}\frac{2}{\left[1+(1.339(2\pi)Lk)^2\right]^{5/6}} \tag{5}$$

For transverse disturbances this spectrum is

$$S_{v,VK}(k) = 2.7\varepsilon^{2/3}L^{5/3}\frac{1+\frac{8}{3}(1.339(2\pi)Lk)^2}{\left[1+(1.339(2\pi)Lk)^2\right]^{11/6}} \tag{6}$$

The main difference of this von Karman form (compared to Kolmogorov model) is that the disturbance spectral levels off at low frequencies. Another difference is that in the von Karman form of the Tank model, the integral length scale, L, is explicitly employed, Equations (5) to (6). The integral length scale is related to the outer scale length, L_o (the length of the atmospheric turbulence patch) by $L=L_o/14.7$ for the longitudinal disturbance, and $L=2L_o/19$ for the transverse disturbance (Soreide and Tank (1996)). Figure 2 shows a plot of the Kolmogorov acoustic wave velocity spectral in (m/sec/Hz) compared to the corresponding von Karman spectral for the longitudinal and transverse acoustic wave velocity disturbances. Different values of L will produce the same curves

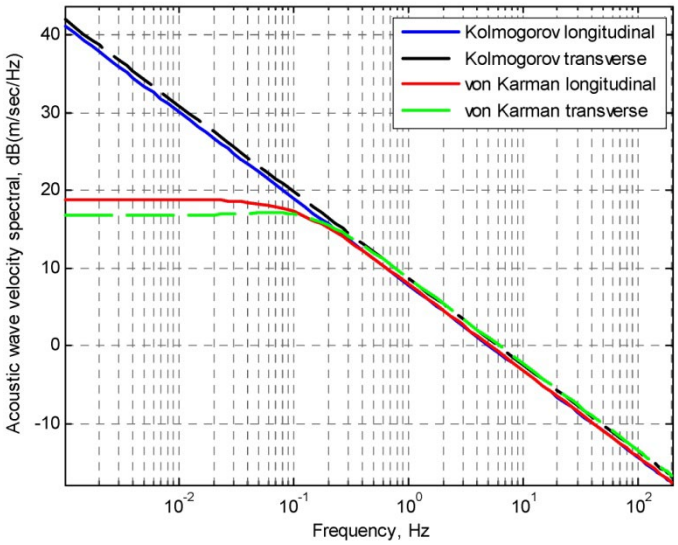

Figure 2.—Acoustic wave velocity spectral comparisons for the Kolmogorov and von Karman spectral.

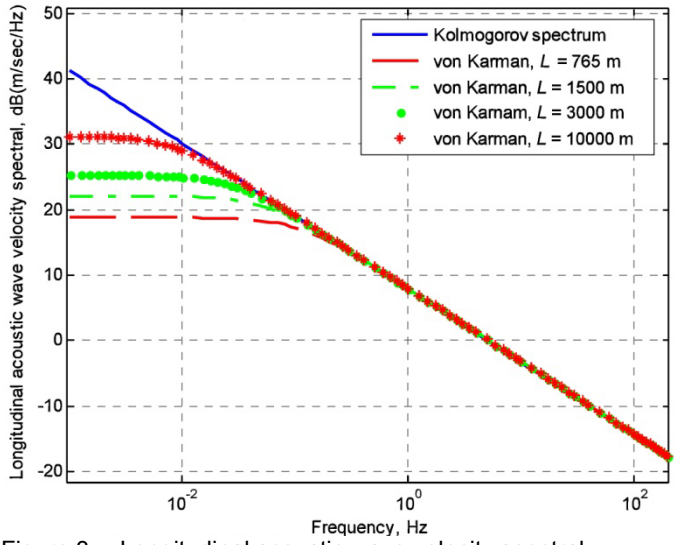

Figure 3.—Longitudinal acoustic wave velocity spectral comparisons between the Kolmogorov and the von Karman forms of four different integral scale lengths.

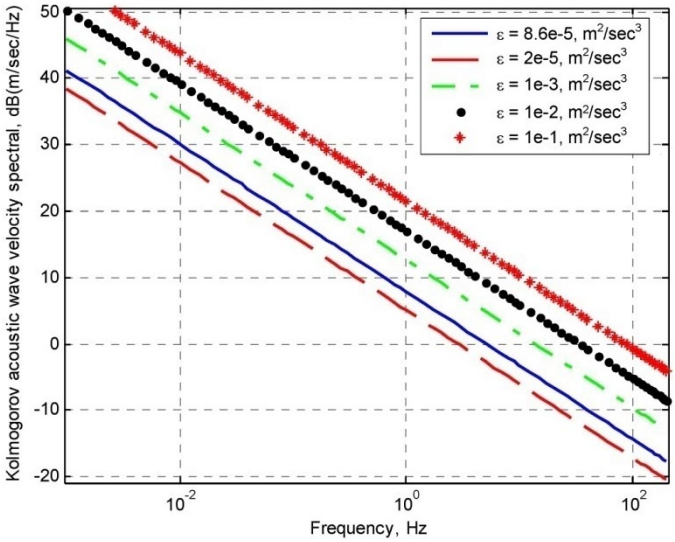

Figure 4.—Longitudinal acoustic wave velocity spectral comparisons for different integral scale lengths.

with either a higher or lower, low-frequency asymptote as shown in Figure 3 for the longitudinal disturbance. For comparison, a value of L=762 m pertains to an atmospheric turbulence patch of approximately 11 km for the longitudinal disturbance, while a value of L=10 km pertains to a turbulence patch of approximately 147 km long. Tank used a value of L=762 m, which he called as standard in the airplane industry. Since a typical control design can sufficiently attenuate disturbance frequencies well beyond 1 Hz, based on Figure 3 differences in the value of L and thereby, differences in the lower frequency asymptote, will have negligible effect on the control design. For completeness, the Kolmogorov spectrum for the longitudinal acoustic wave velocity is shown in Figure 4 for different values of eddy dissipation rates. As can be deduced from Figure 4, orders of magnitude difference in eddy dissipation rate doesn't produce a corresponding appreciable change in the Kolmogorov spectral density. For instance, approximately four orders difference in ε only makes approximately a factor of 8 difference in velocity as

$$S_2(f) = \left(\frac{\varepsilon_2}{\varepsilon_1}\right)^{2/9} S_1(f), \text{ ((m/sec)/Hz)} \tag{7}$$

Where S_1 is a known spectral density with an eddy dissipation rate ε_1, and S_2 is the calculated spectra density for a different eddy dissipation rate ε_2.

Fractional Order Fit of Atmospheric Turbulence Model

Atmospheric turbulence, as shown in Figure 1, and as described by Kolmogorov and the Tank models in Equation (1) and Equations (5) and (6), is fractional order. In Appendix B a circuit analog of the Tank model von Karman form is utilized, which serves as the basis for deriving integer order pole-zero product TF approximations to the fractional order atmospheric disturbances. The reason for the need to derive approximations to the fractional order equations is because of the difficulty of explicitly or numerically solving fractional order differential equations. The reason is fractional order derivatives, unlike integer order derivatives, do not obey the locality law (i.e., the limit theorem), as further explained in Appendix B.

The idea behind the integer order TF approximation for a fractional order TF is as follows (see Fig. C.1): Starting at a frequency near the beginning of the equivalent 3 dB point of the fractional order TF, an integer order TF approximation can be developed symmetrically centered about the fractional order TF, like a descending staircase shape, by interleafing integer order poles and zeros. As the number of steps of this staircase TF approximation increase, the steps become shorter, eventually collapsing to the straight line of the fractional order TF as the number of poles and zeros of this approximation is increased to infinity. For this approach to work, the frequency of the poles and zeros need to be related to the atmospheric disturbance parameters and also be derived in a way such that the staircase TF approximation is symmetrically centered about the fractional order TF.

Based on the fractional order circuit analog of Equations (5) and (6), see Appendix B for detailed derivations, the values for the equivalent capacitance and resistance of atmospheric turbulences are determined as

$$C_t = \frac{1}{\left(a_t \varepsilon^{2/3}\right)^{1/x} (2\pi Ma)} \tag{8}$$

$$R_t = 1.3390(2\pi)\left(a_t \varepsilon^{2/3}\right)^{1/x} L \tag{9}$$

and the corresponding natural frequency is computed as

$$\omega_n = \frac{K_{\omega n}}{R_t C_t} \tag{10}$$

where the adjustment factor $K_{\omega n}$ is 1, but represented in this form in case any adjustments need to be made to the atmospheric disturbance natural frequency.

Utilizing these circuit analog parameters, a time domain disturbance can be derived (see Appendix C for detailed derivations) based on an integer order TF approximation for atmospheric turbulence, given the atmospheric disturbance parameters ε, L, q, t, and r for the units conversion factor (with q=xr; x=5/3 and r=1/3 for acoustic disturbances and ½ for temperature and pressure) as

$$W_{t,o} \cong K_{t,fit} \frac{\prod_{1}^{m_z}\left(s/\omega_{zi}+1\right))}{\prod_{1}^{m_p}\left(s/\omega_{pi}+1\right)} W_t \tag{11}$$

where W_t is series of input sinusoids with unit amplitude frequency components distributed over the frequency range of interest, which is discussed more in Kopasakis (2010) for propulsion system type disturbances. The frequencies of the poles can be computed as

$$\omega_{pi} = \frac{K_{\omega pi}\omega_{Hpi}\prod_{j=1}^{i-1}\left(\omega_{Hpi}/\omega_{pi-j}+1\right)}{10^{\eta(2i-1)q}\prod_{j=1}^{i-1}\left(\omega_{Hpi}/\omega_{zi-j}+1\right)-1} \quad i = 2,3,\ldots,m_p \tag{12}$$

where the first pole is computed as follows

$$\omega_{p1} = \omega_n\left(10^{\eta q}-1\right)^{\frac{1-q}{q}} \tag{13}$$

and the frequencies of the zeros can be computed as

$$\omega_{zi} = \frac{K_{\omega zi}\omega_{Hzi}\prod_{j=1}^{i-1}\left(\omega_{Hzi}/\omega_{zi-j}+1\right)}{10^{-2\eta iq}\prod_{j=1}^{i}\left(\omega_{Hzi}/\omega_{pi}+1\right)-1} \quad i = 1,2,\ldots,m_z \tag{14}$$

For n number of frequency decades desired to be estimated, the number of poles and zeros in the TF approximation can be determined as

$$m_p = (n-1)/\eta \tag{15}$$

$$m_z = m_p - 1 \tag{16}$$

For a desirable pole-zero density pair, ρ_{pz}, per decade to be used to approximate the fractional order disturbance

$$\eta = \frac{1}{2\rho_{pz}} \tag{17}$$

and the terms ω_{Hpi} and ω_{Hzi} in Equations (11) and (12) can be computed as

$$\omega_{Hpi} = \omega_n\left(10^{\eta q(2i-1)}-1\right)^{1/q}, \; i = 2,\ldots,m_p \tag{18}$$

$$\omega_{Hzi} = \omega_n\left(10^{2\eta q i}-1\right)^{1/q}, \; i = 1,2,\ldots,m_z \tag{19}$$

The utility of ω_{Hpi} and ω_{Hzi} are to maintain symmetry, so that the staircase pole-zero approximation is symmetrically located on top of the fractional order TF asymptote. The proportional gains $K_{\omega pi}$ and $K_{\omega zi}$ in Equations (12) and (14) are reserved for final adjustments that may be needed to these frequencies for more closely approximating the fractional order TFs representing atmospheric disturbance.

Longitudinal and Transverse Acoustic Wave Turbulence

The longitudinal and transverse acoustic wave atmospheric disturbances are in the form of pure wind gusts in the axial direction of vehicle motion and in the vertical direction of motion respectively. Based on the fractional order fits determined in Appendix C, using Equations (8) to (19), with q=xr=5/9 (r=1/3), then $K_{t,\text{fit}}$ in Equation (11), based on inspection of Equations (5) and (6), is

$$K_{l,\text{fit}} = \left(5.4\varepsilon^{2/3}L^{5/3}\right)^{1/3} \tag{20}$$

for the longitudinal disturbance, and

$$K_{v,\text{fit}} = \left(2.7\varepsilon^{2/3}L^{5/3}\right)^{1/3} \tag{21}$$

for the transverse disturbance. For n=3 (i.e., the TF fit over the span of 3 decades in frequency), the proportionality factor adjustments to improve these fits have been found to be (Appendix C),

$$\begin{aligned} K_{l,\omega} &= \left[K_{\omega n}; K_{\omega pi}; K_{\omega zi}\right] \\ &= \left[2.4;\ 1\ \ 1\ \ 1/2.4\ \ 1/1.5;\ \ 1\ \ 1\ \ 1\right] \end{aligned} \tag{22}$$

for the longitudinal acoustic wave, and

$$\begin{aligned} K_{v,\omega} &= \left[K_{\omega n}; K_{\omega pi}; K_{\omega zi}\right] \\ &= \left[4.27;\ 1\ \ 1\ \ 1/2.4\ \ 1/1.5;\ \ 1\ \ 1\ \ 1\right] \end{aligned} \tag{23}$$

for the transverse. These TF fits are compared against the Tank von Karman spectral of Equations (5) and (6), with the units conversion exponent *r*, as shown in Figures 5 and 6 for ε=8.6e–5 (m^2/sec^3) and *L*=762 m. As shown in these figures, the fits do a good job in approximating these disturbances. More accuracy can be achieved around the knee of these spectral by increasing the density of pole-zero pairs per frequency decade in this region. A certain inaccuracy at the lower frequencies would be acceptable for a feedback control design, since a typical control design should have no problem attenuating disturbances at this low frequency range.

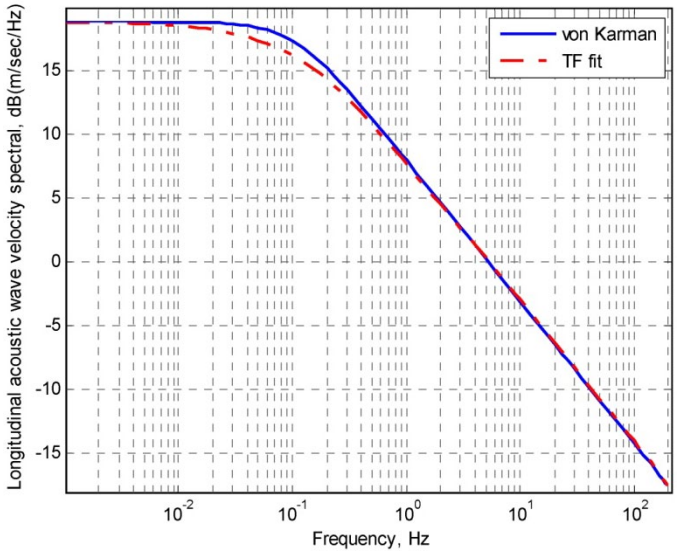

Figure 5.—Longitudinal von Karman spectral, final adjusted TF fit (ε = 8.6e-5 m^2/sec^3, *L* = 762 m).

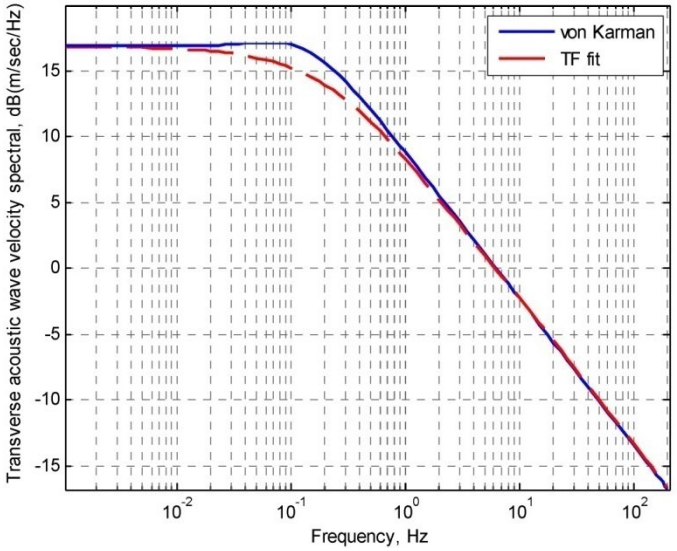

Figure 6.—Transverse von Karman spectral, final adjusted TF fit (ε = 8.6e-5 m^2/sec^3, *L* = 762 m).

Temperature Turbulence

Atmospheric temperature turbulence causes both temperature as well as acoustic velocity disturbances due to the change in the speed of sound. For the most part, temperature disturbances result in vertical displacement of air parcels (so called gravity waves). Therefore, acoustic velocity disturbances caused by temperature will generate vertical wind gusts that add with any transverse acoustic velocity gusts. However, for the propulsion system, according to Ashun (2004), the wing forebody will turn a vertical gust into a longitudinal gust, by multiplying the vertical gust by the conversion factor $(M_\infty - 1)/\sqrt{M_\infty^2 - 1}$. This factor amounts to 0.63 for M_∞ = 2.35, and can be ignored for worst case purposes. However, this conversion factor decreases with speed and can be taken into account, especially at lower supersonic speeds, for longitudinal acoustic gusts due to temperature turbulence. In Appendix B, Section B.2, first the Kolmogorov spectrum of the longitudinal acoustic wave and that of the temperature, based on Equation (1) are plotted (Fig. B.6). This results in parallel spectral lines with frequency, similar to the Kolmogorov spectra shown in Figure 2. Then the von Karman temperature spectral is constructed by scaling the horizontal von Karman type acoustic wave spectral (i.e., scaling it by the difference in magnitudes of these Kolmogorov spectra as shown in Fig. B.6).

Temperature turbulence spectral density, as can be seen in Figure 1, also follows the 5/3 law, but its units are in terms of Kelvin squared. Thus, in order to convert the units to Kelvin, the exponent *r* becomes ½, which makes the fractional order *q*=5/6. Based on this, the TF fit performed for temperature is done the same way as with acoustic wave in the previous section (i.e., utilizing Equations (8) to (19), with the additional relations.

$$K_{T,\mathrm{fit(temp)}} = \sqrt{14.0\varepsilon^{2/3}L^{5/3}} \tag{24}$$

$$\begin{aligned} K_{T,\omega} &= \left[K_{\omega n}; K_{\omega pi}; K_{\omega zi}\right] \\ &= \left[1.5;\ 1\ \ 1\ \ 1/1.1\ \ 1/1.2;\ \ 1\ \ 1\ \ 1\right] \end{aligned} \tag{25}$$

Figure 7 shows this TF fit and the spectral of Equation (5) (i.e., Eq. (5) substituting the scaled Eq. (24) for the numerator and by also applying the units conversion factor in the denominator, for ε=8.6e-5 an *L*=762 m.

The proportionality factors, K_t, for all the fits can also be considered part of the formulations. Their accuracy at higher frequencies starts deviating somewhat with higher values of *L* (integral length scales of few thousand meters and above), values that are considered to be outside the typical range. As discussed before, *L*=762 m is considered standard in airplane industry.

Temperature turbulence also causes acoustic wave gusts due to change of the local speed of sound. By perturbing the relation of the speed of sound and temperature in Equation (3),

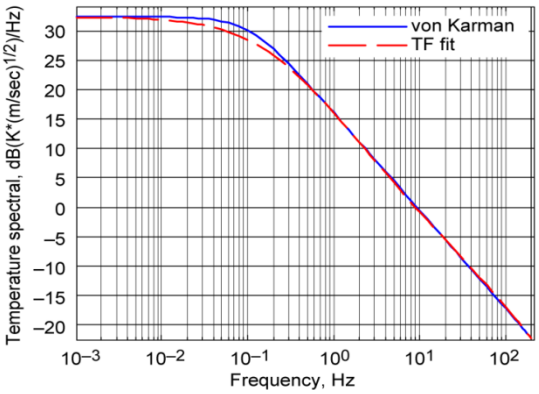

Figure 7.—Temperature von Karman spectral and its TF fit (ε = 8.6e-5 m^2/sec^3, *L* = 762 m).

and substituting the resulting expression for Δa into the Mach number equation of $M=v/a$, the relation between the change in temperature and acoustic velocity can be obtained as

$$\Delta v = \frac{M\gamma R}{2a_o}\Delta T \tag{26}$$

This relation can be applied to Equation (24) to compute $K_{T,\text{fit(acoustic)}}$ for the acoustic wave velocity disturbance due to an atmospheric temperature fluctuation as

$$K_{T,\text{fit(acoustic)}} = \frac{M\gamma R}{2a_o}\sqrt{14.0\varepsilon^{2/3}L^{5/3}} \tag{27}$$

Equation (27) is applicable to transverse or vertical wind gust disturbances generated by temperature turbulence, and accurate in the worst case sense for longitudinal wind gusts, especially at higher supersonic Mach numbers. Generally, longitudinal wind gusts due to temperature variations can be expressed as follows by utilizing the conversion factor $(M_\infty - 1)/\sqrt{M_\infty^2 - 1}$

$$K_{T,\text{fit(longitudinal)}} = \frac{M_\infty(M_\infty - 1)\gamma R}{2a_o\sqrt{M_\infty^2 - 1}}\sqrt{14.0\varepsilon^{2/3}L^{5/3}} \tag{28}$$

This TF fit for the acoustic velocity disturbance at supersonic cruise altitude, at Mach 2.35, for L=762 m and two different values of ε is shown in Figure 8. The TF fit for $\varepsilon=8.6\times10^{-5}$ (m^2/sec^3) and for two different values of integral scale lengths is shown in Figure 9. As can be seen from Figure 8 or Figure 9 compared to Figure 5, the acoustic velocity gusts produced by fluctuations in temperature are much higher in amplitude than those produced by pure acoustic velocity gusts.

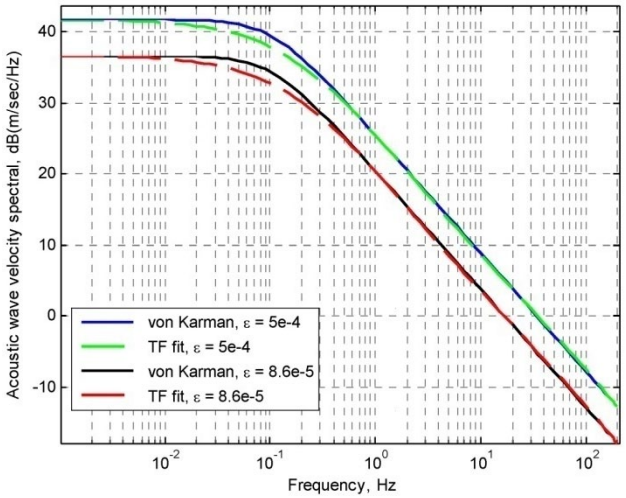

Figure 8.—Von Karman acoustic wave velocity spectral due to temperature gust and its TF fits for different eddy dissipation rates (*L* = 762 m).

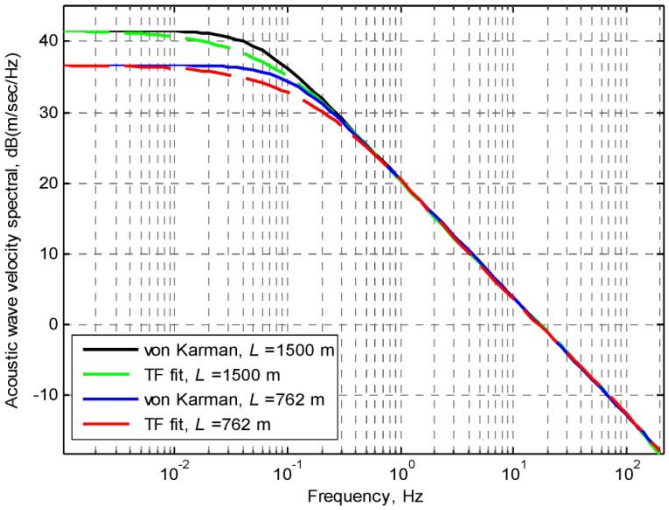

Figure 9.—Von Karman acoustic wave velocity spectral due to temperature gust and its TF fits for different integral scale lengths (ε = 8.6e-5 m^2/sec^3).

As shown in Appendix B, Figure B.8, for the combined acoustic wave, the acoustic wave velocity due to temperature gust dominates in the low frequency range and at higher frequencies both acoustic waves affect the total. At worst case, it can be assumed that both affects of the acoustic wave velocity can combine. It is also assumed that both the longitudinal and transverse acoustic wave velocities will not combine to produce worst case affects. For engines under the wing, the transverse wave is assumed to be converted to a longitudinal wave via the wing forebody (Ahsun (2004)), see Appendix B.

Pressure Turbulence

The longitudinal velocity wave spectral and the pressure spectral of Equation (1) was utilized the same way as described in the previous section for the temperature to scale the von Karman type acoustic wave spectral to come up with the pressure spectral of atmospheric disturbances, see Section B.3. The units conversion exponent for pressure is the same as that for temperature (i.e., r=1/2), which makes the fractional order the same (i.e., q=5/6). As such, $K_{p,\text{fit}}$ and $K_{p,\omega}$ were computed as follows

$$K_{P,\text{fit}} = \sqrt{11.6\varepsilon^{2/3}L^{5/3}} \tag{29}$$

$$\begin{aligned} K_{P,\omega} &= \left[K_{\omega n}; K_{\omega pi}; K_{\omega zi}\right] \\ &= \left[1.5;\ 1\ \ 1\ \ 1/1.1\ \ 1/1.2;\ 1\ \ 1\ \ 1\right] \end{aligned} \tag{30}$$

Figure 10 shows this TF fit for ε=8.6e–5 (m^2/sec^3) and L=762 m compared to the scaled von Karman type spectral—i.e., Equation (29) substituted for the numerator and proportional factor of Equation (5) and the denominator of Equation (5), raised to the power r.

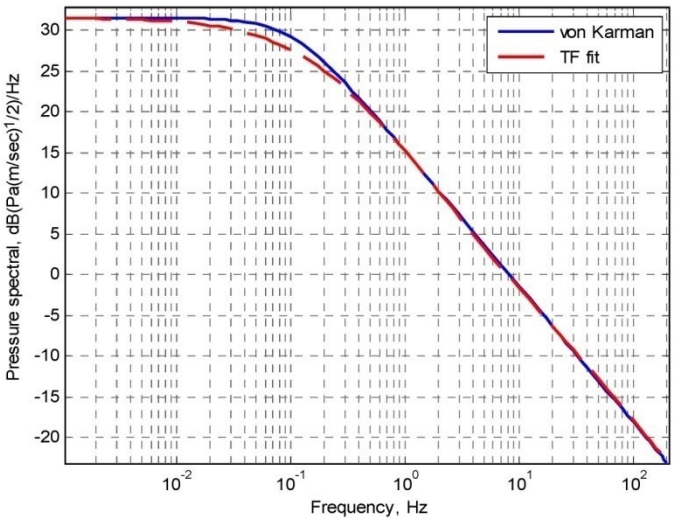

Figure 10.—Pressure von Karman spectral and its TF fit (ε = 8.6e-5 m^2/sec^3, L = 762 m).

Density Turbulence

Density disturbances are contained within temperature and pressure fluctuations and its inclusion in a simulation, along with pressure and temperature will produce unnecessary additional disturbances. However, if need be, the relation of density disturbance with temperature and pressure can be derived as (by perturbing the state equation)

$$\Delta\rho = \frac{P_o + \Delta P}{R(T_o + \Delta T)} - \frac{P_o}{RT_o} \tag{31}$$

A plot of density disturbance utilizing Equation (31) is shown in Figure 11.

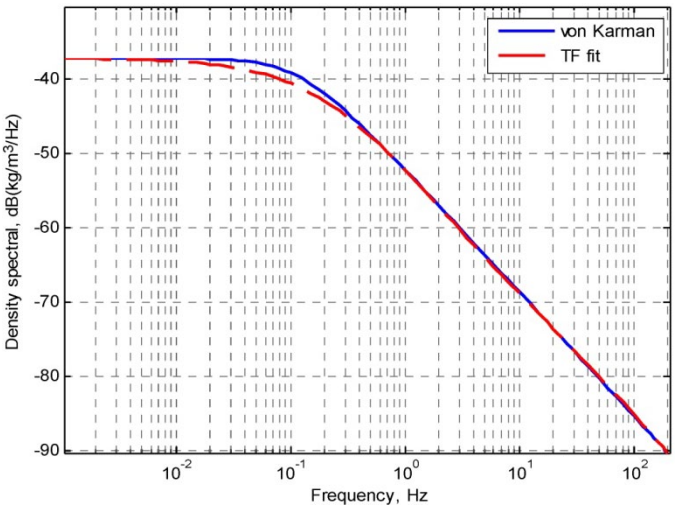

Figure 11.—Density von Karman spectral and its TF fit (ε = 8.6e-5 m^2/sec^3, L = 762 m).

Simplified Atmospheric Turbulence Model for Controls Design

The attempt in this section will be to further simplify the fractional order TF fit developed in the previous sections, by identifying certain characteristics of this model that are important for controls design to handle atmospheric turbulence.

Based on observations, utilizing Figure 8, differences in eddy dissipation rates, ε, produce spectral densities with the same frequencies, offset by a fixed magnitude. This offset is accounted by differences in TF gain. Calculating these frequencies using the formulations developed so far also supports this observation. Differences in the fractional order of the disturbances, such as longitudinal acoustic wave velocity vs. temperature, obviously, will produce different spectral frequencies. Unlike differences in eddy dissipation rates that produce the same frequencies with different TF magnitudes, inspection of Figure 9 shows that spectral with different integral length scales, L, will be represented by different frequencies. However, different integral length scales only affect the low frequency spectral, where a typical feedback controls design should have no difficulty attenuating disturbances at such a low frequency range.

Figure 12 shows spectral density TF fits, first, with a fixed integral length scale and two different values of ε. This shows that the differences in ε produce a fixed offset in magnitude, but with the same pole-zero frequencies. Then Figure 12 also shows comparison between two spectral densities with the same value of ε and two different values of L. This later comparison, with different values of L, is represented with different pole-zero frequencies. However, their high frequency asymptotes match, which means that for the purpose of controls design, either of these TF fits can be utilized, despite their differences in pole-zero frequencies.

Therefore, the frequency domain atmospheric turbulence model can be simplified by utilizing the model developed in the previous section to calculate the fixed frequencies due to a fixed integral length scale and variable eddy dissipation rates. Based on that, the simplified model developed for atmospheric turbulence, which ignores differences in the pole-zero frequencies due to different integral length scales can be represented as

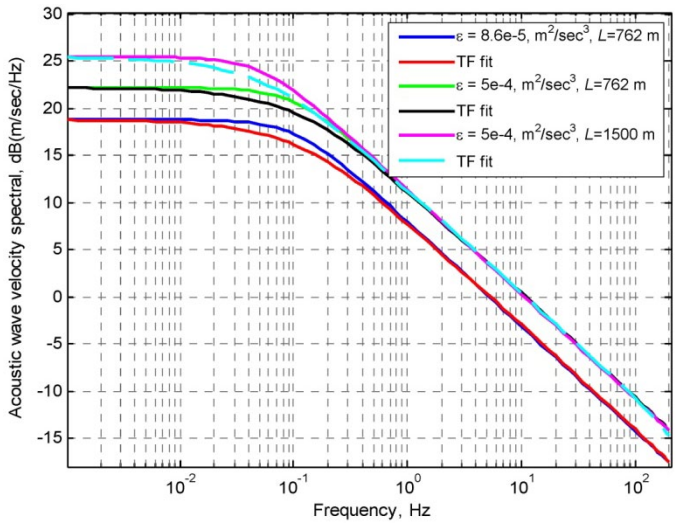

Figure 12.—von Karman longitudinal acoustic wave velocity spectral and its TF Fits due to different values of eddy dissipation rates and Integral Length Scales.

$$G_{LA}(s) = 70\varepsilon^{2/9}\frac{(s/9.2+1)(s/55.0+1)(s/335.5+1)}{(s/1.46+1)(s/30.1+1)(s/85.7+1)(s/1593.1+1)} \tag{32}$$

$$G_{VA}(s) = 56\varepsilon^{2/9}\frac{(s/9.2+1)(s/55.0+1)(s/335.5+1)}{(s/1.46+1)(s/30.1+1)(s/85.7+1)(s/1593.1+1)} \tag{33}$$

$$G_{T}(s) = 943\varepsilon^{2/6}\frac{(s/33.0+1)(s/45.6+1)(s/602.4+1)}{(s/1.1+1)(s/25.1+1)(s/109.8+1)(s/816.3+1)} \tag{34}$$

$$G_{TLA}(s) = 472\varepsilon^{2/6}\frac{(M-1)}{\sqrt{M^2-1}}\frac{M\gamma R}{a_o}\frac{(s/33.0+1)(s/45.6+1)(s/602.4+1)}{(s/1.1+1)(s/25.1+1)(s/109.8+1)(s/816.3+1)} \tag{35}$$

$$G_{TVA}(s) = 472\varepsilon^{2/6}\frac{M\gamma R}{a_o}\frac{(s/33.0+1)(s/45.6+1)(s/602.4+1)}{(s/1.1+1)(s/25.1+1)(s/109.8+1)(s/816.3+1)} \tag{36}$$

$$G_{P}(s) = 859\varepsilon^{2/6}\frac{(s/33.0+1)(s/45.6+1)(s/602.4+1)}{(s/1.1+1)(s/25.1+1)(s/109.8+1)(s/816.3+1)} \tag{37}$$

Where G_{LA}, G_{VA}, G_T, G_{TLA}, G_{TVA} and G_P are the simplified atmospheric disturbance TF for longitudinal and transverse acoustic wave velocity, temperature, longitudinal and vertical acoustic velocities due to temperature, and pressure respectively. The factor $(M_\infty - 1)/\sqrt{M_\infty^2 - 1}$ in Equation (35) can be set to one for worst case turbulence conditions, especially for relatively high Mach numbers, in which case it makes Equation (35) and Equation (36) the same.

The TF fit described in the previous section was carried up to 200 Hz, which should make it accurate even beyond this frequency range. However, the model simplification represented by Equations (30) to (34) introduces additional error at high frequencies and its validity should be limited to about 200 Hz. The frequencies of this model are based on an integral length scale of L=762 m. This means that this simplified model is not unique, and other equivalent models can be calculated using different values of L with the equations developed in the previous sections. Thus, for a controls design, which can adequately attenuate 1 Hz disturbances, this model is accurate for values of L as low as 100 m, which is well below the expected range of L. A value of L=762 m is considered standard in the airplane industry as mentioned before.

Time Domain Disturbances

The TF fits in the previous section can be thought as filters, which take input disturbances at desirable frequencies and

convert them to representative free stream atmospheric disturbances. The TF fits contain the representative magnitudes of these disturbances. Thus, the discrete time domain frequencies, W_t, only need to have unity RMS values. For instance, a time domain input can be constructed as a sum of unit amplitude sinusoids, starting with a low frequency, somewhere at the low frequency asymptote of the spectral, and continuing up with sinusoids that are dispersed along the high frequency asymptote up to frequencies that covers the controller bandwidth. Also, the control design can be checked with single frequency sinusoids, sequentially simulated. Of course, the total energy or the maximum amplitude of the disturbance will need to be reasonable. For instance, it may be considered that total wind gust will not exceed an amplitude of 180 mph, or some other reasonable number that depends on altitude. For more information on propulsion type disturbance considerations, see Kopasakis (2010).

For most of the spectral density simulations covered so far, the worst case eddy dissipation rate for low to moderate turbulence was used for altitudes of about 36,000 ft (~11 km) and above. However, the highest atmospheric turbulence ever recorded had an eddy dissipation rate of 1.7e-3 (m^2/sec^3) (Tank (1994)). Theoretically, it is possible that even more severe turbulence can be encountered according to McMinn (1997). McMinn provides tables for altitudes, turbulence severity, and associated eddy dissipation rates. Kopasakis (2010) covers more in this area of simulating atmospheric disturbances, including considerations for atmospheric turbulence specifications. Fairall (1991) also covers implementation of time domain sinusoidal input disturbances by utilizing Fourier sinusoids.

As mentioned before, previous works cover atmospheric turbulence probabilistically, as an *exceedance* for controls design purposes. In terms of probabilistic atmospheric turbulence models, there are no comparisons drawn here between those models and the non-probabilistic approach described in this paper, even though exceedance can also be incorporated with this approach. The modeling approach developed in this paper is geared towards implementing controls design by considering worst case atmospheric turbulence. This also allows implementation of control designs to cover worst case turbulence encounters, without penalizing performance under normal atmospheric conditions, by incorporating control scheduling in the design.

Figure 13 shows a time domain longitudinal acoustic wave disturbance utilizing the acoustic wave TF fit discussed in the previous section. The input to this TF is a combination of unity amplitude sinusoids distributed along the frequency range shown in Figure 5. For a single unity amplitude sinusoid at low frequency, the amplitude of the acoustic disturbance would be approximately 9 m/sec according to Figure 5. For this summation of unity amplitude input sinusoids, their amplitudes combine to give approximately 15 m/sec maximum disturbance. The same approach can be used to construct other atmospheric disturbances for time domain simulations.

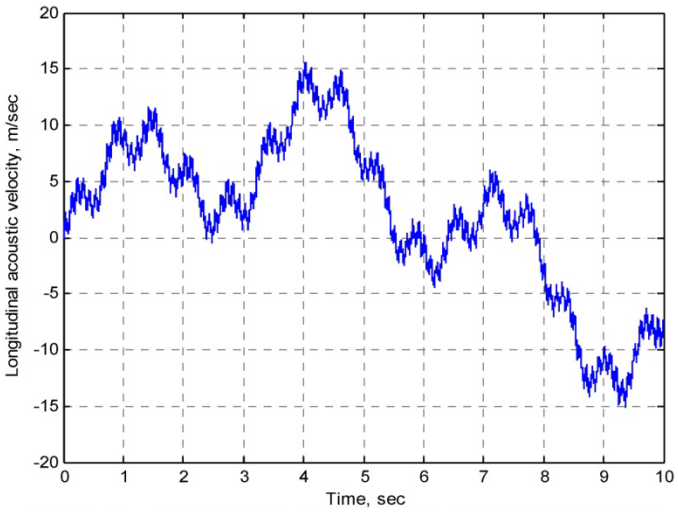

Figure 13.—Longitudinal acoustic wave velocity disturbance created using the TF fit of the longitudinal acoustic wave with unity input sinusoids.

In Kopasakis (2010), considerations for atmospheric turbulence specifications are provided, with more discussion on the frequencies of these turbulences, also involving the vehicle Mach number. In this reference a control design example is also provided for the supersonic inlet shock control problem, in the presence of atmospheric turbulence.

Conclusion

In this paper derivations were carried out to approximate the fractional order atmospheric turbulence with integer order pole-zero transfer function fits for more accurate time domain simulations. An existing von Karman type model form of the Kolmogorov spectral is utilized initially for the acoustic velocity gusts disturbances. This model is scaled in this paper in order to also develop the von Karman model forms for other type of atmospheric disturbances like temperature, pressure, and density. Because of the fractional order of these models, a circuit equivalent is developed that is used as the basis to derive the integer order pole-zero approximations. Utilizing the formulations presented in this paper, the transfer function poles and zeros of the approximations to the atmospheric disturbances can be directly computed for different parameters describing atmospheric turbulence. The model is derived to duplicate the fractional order form of atmospheric turbulence and is more accurate than previous models developed. These new models could be used to design controls for aerospace vehicle propulsion or flight control systems.

Appendix A.—Nomenclature

a	speed of sound, (m/sec)
a_o	ambient speed of sound, (m/sec)
C_t	equivalent electric circuit capacitance for t-type of disturbance, (farads)
f	frequency, (Hz)
f_n	natural frequency, (Hz)
f_c	frequency of computed correction factor, (Hz)
h	altitude, (km)
H	vector of intersection points to match estimated and fractional order TFs
k	wavenumber, (rad/m) or (cycles/m)
K	proportional gains
K_t	von Karman horizontal asymptote for t-type of disturbance
$K_{\omega n}$	adjustment factor to disturbance natural frequency
l	length, (m)
L	integral length scale, (m)
L_o	outer scale length, (m)
m_p	number of poles in the TF approximation
m_z	number of zeros in the TF approximation
M	mach number
n	number of frequency decades desired to estimate the fractional order TF
P	pressure, (Pa)
P_o	standard atmospheric pressure, (Pa)
q	fractional order of equivalent electrical circuit
R	universal gas constant, 287 (N*m)/(kg*K)
r	units conversion exponent of atmospheric disturbance
R_t	equivalent electric circuit resistance for t-type of disturbance, (ohms)
S	atmospheric turbulence spectral density
$S_{l\text{-or-}v}$	atmospheric velocity turbulence spectral density, $(m^3/sec^2)/(rad)$ or $(m/sec)^3/(Hz)$ also converted to (m/sec)/(Hz) by taking 1/3 root
s	Laplace operator
T	temperature, (K)
T_o	standard atmospheric temperature, (K)
T_{oh}	temperature at an arbitrary reference height, (K)
v	flow velocity, (m/sec)
v_l'	velocity fluctuation in a region of size l of the basic laminar flow, (m/sec)
W	unity disturbance time domain signal
W_t	disturbance time domain signal for t-type of disturbance
x	fractional order of atmospheric disturbance spectral

A.1 Greek

α	constant associated with atmospheric turbulence spectral density
α_l	longitudinal, (unit less),
α_v	transverse or vertical, (unit less)
α_T	temperature, $(°K^2sec^2m^{-2})$
α_P	pressure, $(Pa^2sec^2m^{-2})$
γ	ratio of specific heats, ($\gamma = 1.41$)
ε	eddy dissipation rate, (m^2/sec^3)
η	the ratio of each decade interval where a pole or a zero will be used to estimate the fractional order TF
λ	wave length of atmospheric disturbance (m/cycle)
ν	kinematic viscosity of a laminar flow, (m^2/sec)
ρ	weight density, (kg/m^3)
ρ_{pz}	density of pole-zero pairs per decade for estimated TF
ω_n	natural frequency, (rad/sec)
ω_{pi}	frequency of TF pole i of integer order approx. (rad/sec)
ω_{zi}	frequency of TF zero i of integer order approx. (rad/sec)

A.2 Subscripts

a	constant associated with circuit capacitance correctional factor
A	variable associated with an adjustment
C	constant associated with circuit capacitance correctional factor
H	associated with symmetry frequencies for the approx.
fit	variable associated with TF fit or approximation
l	variable associated with longitudinal atmospheric disturbance
LA	variable associated with longitudinal acoustic disturbance
VA	variable associated with vertical or transverse acoustic disturbance
P	variable associated with pressure disturbance
t	variable associated with type of disturbance
T	variable associated with temperature disturbance
TLA	variable associated with longitudinal acoustic disturbance due to temperature

TVA	variable associated with vertical or transverse acoustic disturbance due to temperature
v	variable associated with vertical or transverse atmospheric disturbance
VK	variable associated with the von Karman spectral density
VKA	variable associated with the von Karman spectral density circuit approximation
o	variable associated with an output
p	variable associated with TF poles
s	variable associated with a static quantity
z	variable associated with TF zeros
ω*pi*	variable associated with pole frequencies
ω*zi*	variable associated with zero frequencies
∞	variable associated with freestream conditions

Appendix B.—Circuit Analog of the von Karman Model Form

In this appendix the von Karman approximations to the different atmospheric disturbances based on the Kolmogorov spectrum given by (Soreide and Tank (a) and (b)) are approximated by utilizing an electrical circuit analog. The purpose of the circuit analog is to serve as basis for deriving integer order pole-zero product TF approximations to the fractional order atmospheric disturbances. The reason for the need to derive approximations to the fractional order equations is because of the difficulty of numerically solving fractional order differential equations. For instance, unlike integer order, fractional order derivatives obey the law of non-locality. This property of fractional order derivatives makes the state transition matrix a convolution integral, with each integration step necessitating the computation of the convolution of the state all the way back to time zero where the state had an initial value of zero.

B.1 Longitudinal and Transverse Disturbances

The Kolmogorov atmospheric turbulence spectral model as described in the main body, Equation (1), of this paper is

$$S_t(k) = \alpha_t \varepsilon^{2/3} k^{-5/3} \tag{B.1}$$

And the von Karman longitudinal and transverse models respectively, reproduced from Equations (5) and (6) from the main body of this report are:

$$S_{l,VK}(k) = 2.7\varepsilon^{2/3} L^{5/3} \frac{2}{\left[1+(1.339(2\pi)Lk)^2\right]^{5/6}} \tag{B.2}$$

$$S_{v,VK}(k) = 2.7\varepsilon^{2/3} L^{5/3} \frac{1+\frac{8}{3}(1.339(2\pi)Lk)^2}{\left[1+(1.339(2\pi)Lk)^2\right]^{11/6}} \tag{B.3}$$

The shape of the von Karman spectrum approximations of Equations (B.2) and (B.3) is that of a parallel network consisting of a resistive element corresponding to the horizontal von Karman asymptote and capacitive element corresponding to the high frequency Kolmogorov asymptote as

$$S_{t,VKA}(k) = \frac{\left[K_t S_t(k)\right]^r}{(K_t)^r + S_t^r(k)}, \text{ (m/sec)/Hz} \tag{B.4}$$

Where r represents the units conversion exponent from $(\text{m/sec})^3/\text{Hz}$ to (m/sec)/Hz (i.e., r=1/3 in this case—for the longitudinal and transverse acoustic wave disturbances).The variable $S_t(k)$ signifies the Kolmogorov spectrum of Equation (B.1) or the high-frequency asymptote of the von Karman spectrum, and K_t, signifies the von Karman low-frequency asymptote or TF gain for the type of disturbance of Equations (B.2) and (B.3) as

$$K_l = 5.4\varepsilon^{2/3} L^{5/3} \tag{B.5}$$

$$K_v = 2.7\varepsilon^{2/3} L^{5/3} \tag{B.6}$$

Equation (B.4), for a flow, such as that of the acoustic velocity spectral, is equivalent to a circuit as shown in Figure B.1. The K_t element is a gain for the type of disturbance and is a function of the parameters describing the atmospheric disturbance. The parameter W_t represents an input flow and $W_{t,o}$ represents the resulting output flow, where the exponent q represents the fractional order of these elements. The circuit is an analog of this representation, acting as a disturbance source connected to a filter, meant to be connected to a sink or a system simulation in order to establish an output flow. Applying circuit theory, the TF of this circuit can be computed as

$$W_{t,o} = \frac{K_t^r}{(R_t C_t s)^q + 1} W_t \tag{B.7}$$

Where W_t in the circuit stands for a unity flow signal representing the atmospheric disturbance, containing the disturbance frequencies of interest. More on that will be discussed later. The output signal, $W_{t,o}$, will be the time domain signal representing the von Karman spectral approximation. The subscript t stands for the type of disturbance as before, the exponent q represents the fractional order of the circuit, and the factor K_t is given by Equation (20) or (21). Where $1/(C_t s)^q$ and R_t^q are the capacitive and resistive impedances of the circuit, with s representing the *Laplace* operator.

The values of resistance R_t, capacitance C_t, and the fractional exponent q remain to be determined. The natural frequency of this circuit, ω_n, can be directly obtained by inspection of the TF of Equation (B.7). This frequency will coincide with the frequency at which the low-frequency asymptote (Figs. 2 and 3) intersects the high-frequency asymptote associated with the Kolmogorov spectral or the capacitive impedance of the circuit as

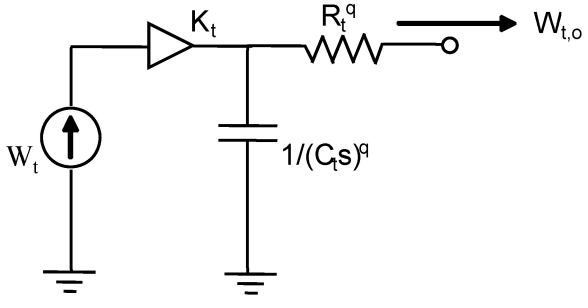

Figure B.1.—Equivalent circuit TF of atmospheric disturbance.

$$\omega_n = \frac{K_{\omega n}}{R_t C_t} \tag{B.8}$$

For now $K_{\omega n}$ is used as a placeholder in case any adjustments are needed to this natural frequency and its value here is set to 1.

In Equation (B.1), k stands for the wavenumber and it is related to the frequency of the disturbance as

$$f = \frac{Ma}{\lambda} = kMa \tag{B.9}$$

For the circuit analogy, the natural frequency of the circuit should be set to the same as that for the von Karman spectral of Equations (B.2 and B.3). By inspection, the natural frequencies of both the von Karman longitudinal and transverse disturbances are the same and can be calculated by substituting Equation (B.9) for f into Equation (B.2) or (B.3) to obtain the relationship

$$\frac{s}{\omega} = 1.339(2\pi)L\frac{f}{Ma}. \tag{B.10}$$

Then by substituting the magnitude s for $2\pi f$ on the right hand side of Equation (B.10) and also setting $\omega_n = 2\pi f_n$ on the left hand side, we can solve for the natural frequency as

$$f_n = \frac{Ma}{1.339(2\pi)L} \tag{B.11}$$

Additionally, the TF of Equation (B.7) needs to represent the von Karman approximation of the Kolomogorov model (i.e., the Kolmogorov asymptote). However, the Kolomogorov model, as a straight line decreasing with frequency in a log scale, can be represented in Figure B.1 with a capacitive impedance. Thus, Equation (B.1) must be this capacitive impedance. This capacitive impedance is raised to the r=1/3 power to account for the units change from (m^3/(sec^2cycle)) to (m/sec)/Hz. Therefore, taking Equation (B.1) and raising it to the power r, replacing k with $f/(Ma)$ using Equation (B.9), then multiplying both numerator and denominator by $(2\pi)^{(5/3)r}$, and by setting the resulting equation to $1/(C_t s)^q$, the following expression can be obtained.

$$\frac{1}{(C_t s)^q} = \left(\frac{\alpha_t \varepsilon^{2/3} (2\pi Ma)^{5/3}}{(2\pi f)^{5/3}} \right)^r \tag{B.12}$$

By inspection of Equation (B.12), since $|s| = 2\pi f$, then $q = (5/3)r$ or in general $q=xr$ (i.e., with x=5/3 in this case), then the capacitance, C_t, can be computed as

$$C_t = \frac{1}{\left(a_t \varepsilon^{2/3}\right)^{1/x} (2\pi Ma)} \tag{B.13}$$

Plugging Equations (B.11) and (B.13) into (B.8), with $\omega = 2\pi f$, R_t can be solved as

$$R_t = 1.339(2\pi)\left(a_t \varepsilon^{2/3}\right)^{1/x} L \tag{B.14}$$

Neither the capacitance C_t nor the resistance R_t depends on the exponent r, utilized for units conversion, which could be indicative of the fundamental nature of these parameters.

With this analysis, the circuit elements for the longitudinal and transverse von Karman model approximations, pertaining to Equation (B.7) have been computed. Figures B.2 and B.3 show the von Karman longitudinal and transverse spectral of Equations (B.2) and (B.3) respectively and their circuit approximation of Equation (B.7). These approximations can be improved by increasing the magnitude of the circuit approximation (K_t in Equation (B.7) for the longitudinal wave in order to reduce the high frequency asymptote error at the lower frequency.

To do this, an offset dB level is chosen (ΔdB) so that the resultant horizontal asymptote of the circuit approximation is not too high above the corresponding horizontal asymptote of the von Karman spectral. This can be done by multiplying Equation (B.7) by a proportional gain K_a, corresponding to this ΔdB level, as $K_a = 10^{\Delta dB/20}$. However, doing that will also raise the high frequency asymptote of the circuit approximation by the same dB level. To counter this affect, the high frequency asymptote can be lowered by the same amount. Lowering the high frequency asymptote can be done by lowering the capacitive impedance, since, the capacitive impedance is inversely proportional to the capacitance, see the circuit in Figure B.1. Thus, this will also require multiplying the capacitance by the same proportional gain, K_a.

For the transverse approximation, illustrated in Figure B.3, it is seen that the high frequency asymptotes of the circuit approximation runs in parallel with the von Karman Spectral. Therefore, the asymptote corresponding to the transverse

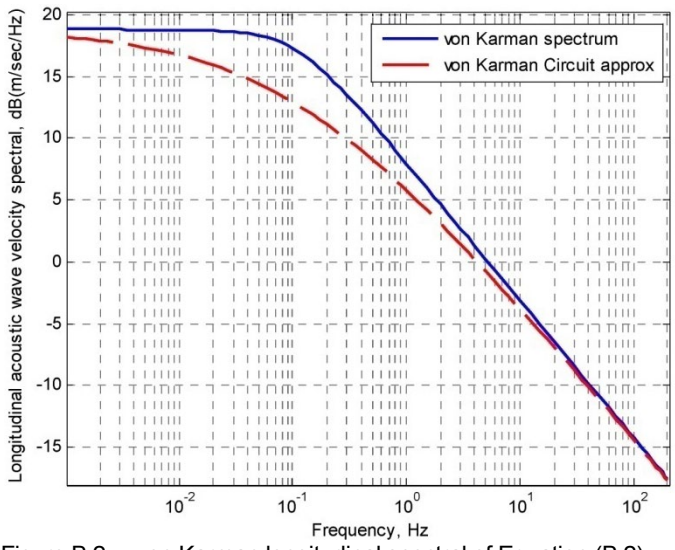

Figure B.2.—von Karman longitudinal spectral of Equation (B.2) and their respective circuit TF approximation of Equation (B.7), (ε = 8.6e-5 m^2/sec^3, L = 762 m).

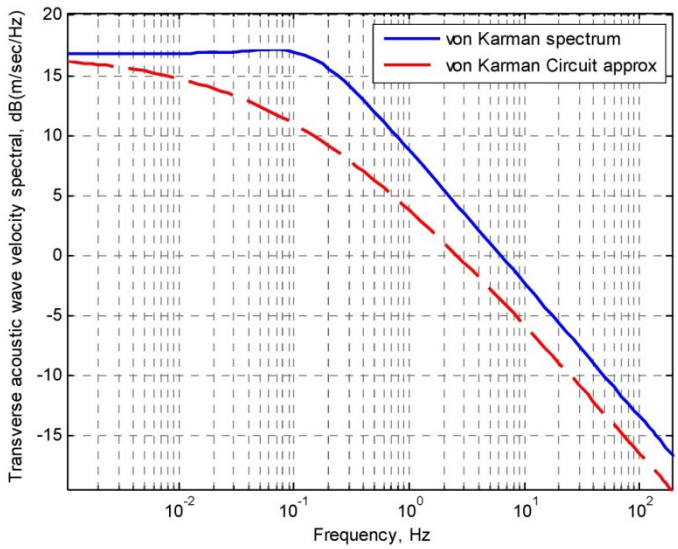

Figure B.3.—von Karman transverse spectral of Equation (B.3) and their respective circuit TF approximation of Equation (B.7) (ε = 8.6e-5 m^2/sec^3, L = 762 m).

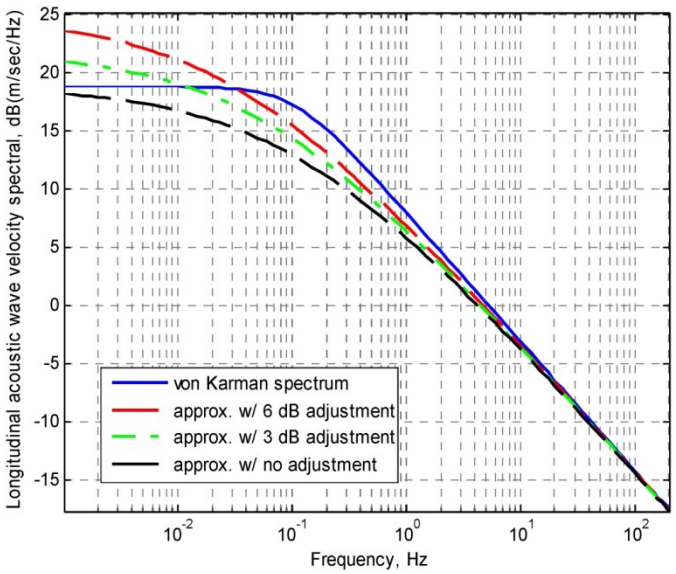

Figure B.4.—Von Karman longitudinal acoustic wave spectral of Equation (B.2) and their circuit TF approximations with different magnitudes of adjustment (ε = 8.6e-5 m^2/sec^3, L = 762 m).

approximation needs to first be raised by doing the reverse of what was done to the capacitance in the previous step (i.e., multiplying the capacitance by the reciprocal of a certain correction factor, K_c. Secondly, the magnitude of the transverse approximation can be adjusted upwards by a desired level, K_a, by performing the two steps described for the adjustment of the longitudinal approximation. These correction factors can be computed as follows.

$$K_{t,a} = 10^{\Delta dB/20} \quad \text{(desired } \Delta dB \text{ level may range from 0 to 6 dB)} \tag{B.15}$$

$$K_{l,c} = 1,\ K_{v,c} = S_{v,VK}(f_c) - W_{v,o}(f_c), \tag{B.16}$$

where f_c is the frequency where this correction factor is to be computed. With these factors computed, Equation (B.13) for the capacitance can be modified utilizing Equations (B.15) and (B.16). But the approach would be to keep the values of the capacitance and resistance generic and instead incorporate these adjustment factors directly into Equation (B.7) as

$$W_{t,oA} = \frac{K_{t,A}}{\left(\left(\frac{K_{t,a}}{K_{t,c}}\right)^{1/q} R_t C_t s\right)^q + 1} W_t \tag{B.17}$$

where

$$K_{t,A} = K_{t,a} K_t^r \tag{B.18}$$

and K_t^r (for the type of disturbance) comes from Equations (B.5) and (B.6) raised to the power r.

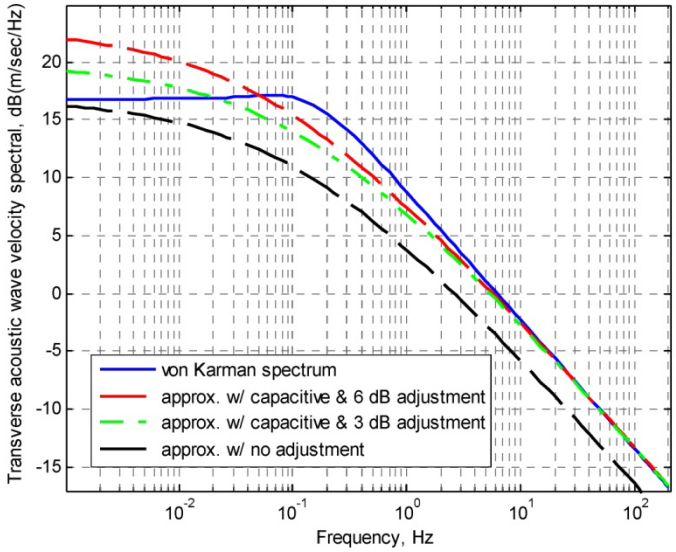

Figure B.5.—Von Karman transverse acoustic wave spectral of Equation (B.3) and their circuit TF approximations with different magnitudes of adjustment (ε=8.6e-5 m^2/sec^3, L=762 m).

Figures B.4 and B.5 show the longitudinal and transverse acoustic wave spectral for the von Karman forms of Equations (B.2) and (B.3) and the equivalent circuit adjustments based on Equation (B.17) for different magnitude adjustments. The $K_{t,a}$ values for these adjustments are based on Equation (B.15). The $K_{v,c}$ value used is 1.424. As discussed before, the important frequencies to match are the higher frequencies, above 1 Hz, because a typical control system design should have no problem attenuating disturbances at the lower frequencies. Therefore, the 6 dB or even the 3 dB, adjustments would normally provide sufficient approximations to the von Karman spectral.

B.2 Temperature Disturbance

Unlike the von Karman model forms of Equations (B.2) and (B.3) for the acoustic wave given by Soreide and Tank (1996), no comparable models exist for temperature, temperature generated acoustic wave, pressure, or density disturbances. Thus the approach here is to utilize the Kolmogorov spectral of Equation (B.1) for the acoustic wave disturbance and compute the differences from that and those of the Kolmogorov Spectral of Equation (B.1) for temperature. Then scale the respective von Karman models of Equations (B.2) and (B.3) by these differences to generate the von Karman models for temperature, pressure and density.

Figure B.6 shows this scaling, with the resulting von Karman spectral for the temperature disturbance. This scaling can be done by graphically finding or by computing the difference in dB magnitude (at any frequency using Equation (B.1)) between the Kolmogorov temperature and the Kolmogorov longitudinal spectral, and then multiplying the von Karman longitudinal spectral by this scale factor (corresponding to the difference in dB magnitude) to come up with the von Karman temperature spectral. As a result, the von Karman temperature spectral is computed as

$$S_{T,VK}(k) = 7.0\varepsilon^{2/3}L^{5/3}\frac{2}{\left[1+(1.339(2\pi)Lk)^2\right]^{5/6}}, \quad \left((\mathrm{K}^2 * \mathrm{m/sec})/\mathrm{Hz}\right) \tag{B.19}$$

The horizontal asymptote for this spectral, based on Equation (B.19), is

$$K_T = 14.0\varepsilon^{2/3}L^{5/3} \tag{B.20}$$

The circuit approximation for this model is similar to that of Equation (B.17), except for some differences in the proportional gains and the fractional exponent as

$$W_{T,oA} = \frac{K_{T,A}}{\left(\left(\frac{K_{T,a}}{K_{T,c}}\right)^{1/q} R_T C_T s\right)^q + 1} W_T \tag{B.21}$$

Where $K_{T,a}$ is the same as Equation (B.15) for the desired adjustment and

$$K_{T,A} = K_{T,a}K_T^r, \; K_{T,c} = 1 \tag{B.22}$$

As before, the fractional exponent is $q=xr$. However, this time for the temperature disturbance, the units conversion exponent is $r=1/2$ (see Fig. 1 for the temperature units). As such, the fractional exponent for temperature is $q=5/6$, instead of $q=5/9$ for the acoustic wave disturbances. Figure B.7 shows a plot of the circuit approximation for temperature based on Equation (B.21), with $K_{T,a}$ = 1.4125 (i.e., raising the circuit approximation magnitude by 3 dB) , compared to its scaled von Karman spectral of Equation (B.19).

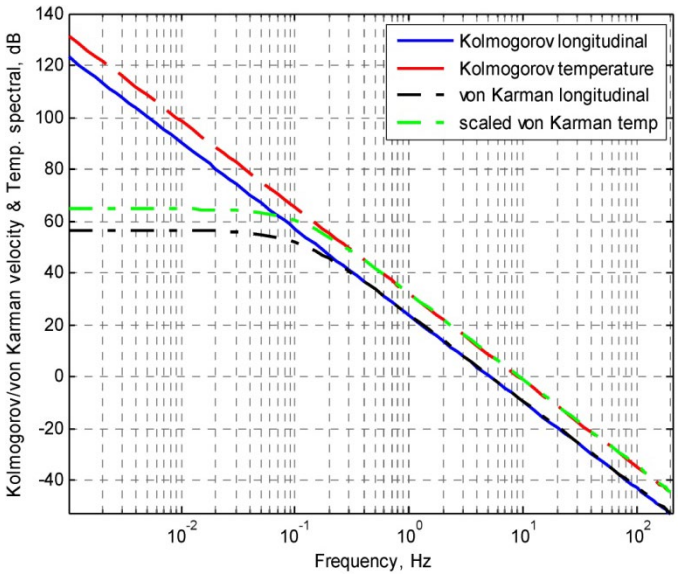

Figure B.6.—Kolmogorov spectral of the longitudinal wave and temperature and scaling of the longitudinal von Karman spectral to come up with the von Karman temperature model form (ε = 8.6e-5 m^2/sec^3, L = 762 m).

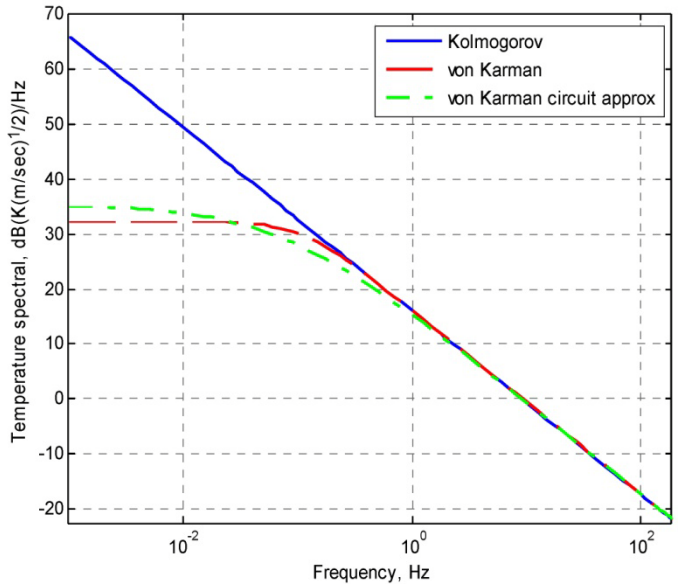

Figure B.7.—Kolmogorov and von Karman spectral for temperature and its von Karman circuit approximation (ε = 8.6e-5 m^2/sec^3, L = 762 m).

By perturbing the relation of the speed of sound and temperature, $a = \sqrt{\gamma RT}$, and substituting the resulting expression for Δa into the Mach number equation of $M=v/a$, the relation between the change in temperature and acoustic velocity can be obtained as

$$\Delta v = \frac{M\gamma R}{2a_o}\Delta T \qquad \text{(B.23)}$$

Where γ is the ratio of specific heats (~1.41), R is the universal gas constant (~287 – N*m/(kg*K)), and a_o is the standard speed of sound at that altitude (~ 295 m/sec at supersonic cruise altitude). Figures B.8 and B.9 show the von Karman spectral for the longitudinal and transverse acoustic waves respectively, the temperature gust based on Equation (B.19) turned to either longitudinal or vertical acoustic wave velocity gust, and the combination of the two. As shown in these figures, for the combined acoustic wave the acoustic wave velocity due to temperature gust dominates in the low frequency range. At higher frequencies, both affect the total and the resultant slope is more of a combination of the two disturbances. The question in encountering atmospheric turbulence is if it's possible that the two effects (i.e., the acoustic wave due to pure wind gusts and acoustic wave disturbance due to a temperature fluctuation) can combine at the same time to produce worst case conditions. As for longitudinal and transverse disturbances combining, in terms of the propulsion system, the assumption is that the longitudinal disturbance would be the worst case (i.e., the longitudinal and the transverse or vertical would not combine at the same time). This is especially true for propulsion systems located under the wing, since, the vertical acoustic wave loses some velocity when it's turned to a longitudinal acoustic gust via the vehicle wing forebody (Ahsun (2004)).

B.3 Pressure Disturbance

For an atmospheric pressure disturbance, as discussed in the previous section, the Kolmogorov spectral of Equation (B.1) will be used to come up with the von Karman model form by scaling the respective models of the longitudinal acoustic wave disturbance. Figure B.10 shows this scaling, with the resulting von Karman spectral for the pressure disturbance. As a result, the von Karman pressure spectral is computed as

$$S_{P,VK}(k) = 5.8\varepsilon^{2/3}L^{5/3}\frac{2}{[1+(1.339(2\pi)Lk)^2]^{5/6}}, \quad \left(\left(\text{Pa}^2 * \text{m/sec}\right)/\text{Hz}\right) \qquad \text{(B.24)}$$

The horizontal asymptote for this spectral, based on Equation (B.24), is

$$K_P = 11.6\varepsilon^{2/3}L^{5/3} \qquad \text{(B.25)}$$

Similar to the Temperature spectral, the circuit approximation for this model is the same as that of Equation (B.17), except for some differences in the proportional gains as

$$W_{P,oA} = \frac{K_{P,A}}{\left(\left(\frac{K_{P,a}}{K_{P,c}}\right)^{1/q} R_P C_P s\right)^q + 1} W_P \qquad \text{(B.26)}$$

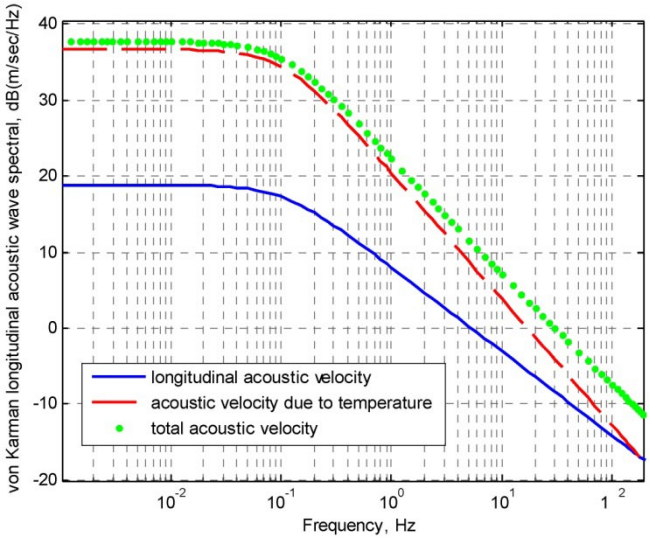

Figure B.8.—Von Karman longitudinal acoustic wave spectral, temperature disturbance turned to acoustic velocity, and the two combined.

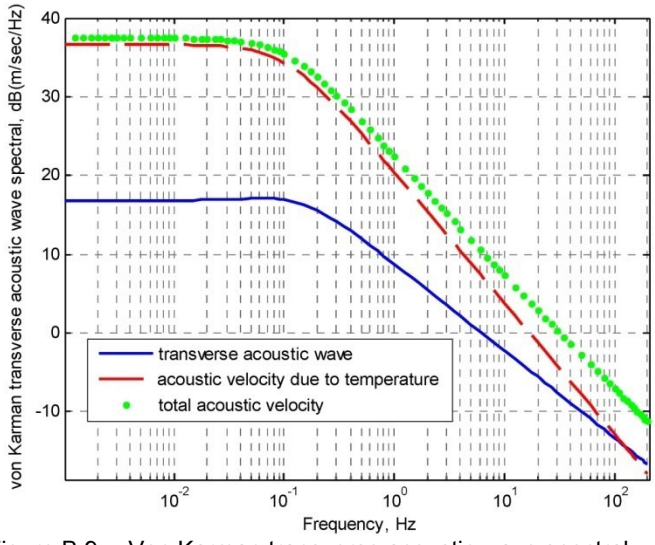

Figure B.9.—Von Karman transverse acoustic wave spectral, temperature disturbance turned to acoustic velocity, and the two combined.

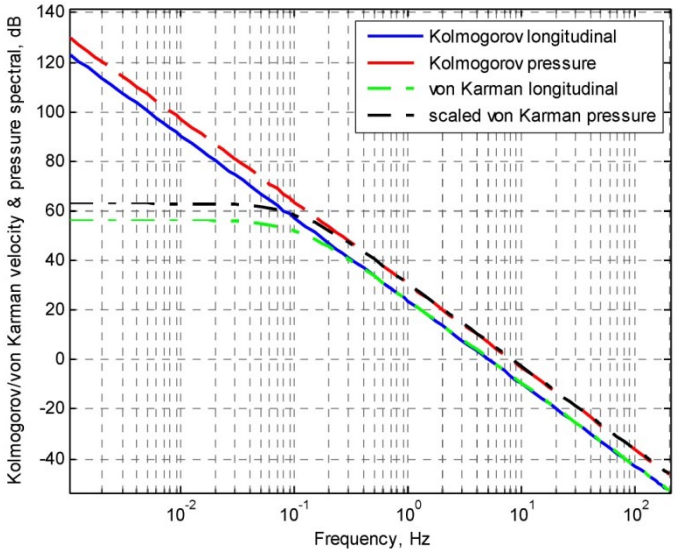

Figure B.10.—Kolmogorov spectral of the longitudinal wave and pressure and scaling of the longitudinal von Karman spectral to come up with the von Karman pressure model form (ε = 8.6e-5 m^2/sec^3, *L* = 762 m).

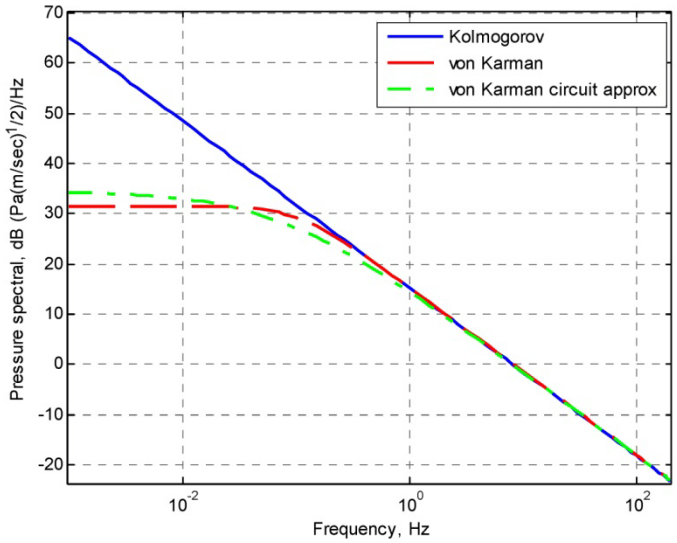

Figure B.11.—Kolmogorov and von Karman spectral for pressure and its von Karman circuit approximation, (ε = 8.6e-5 m^2/sec^3, *L* = 762 m).

Where $K_{P,a}$ is the same as Equation (B.15) for the desired adjustment and

$$K_{P,A} = K_{P,a} K_P^r, \quad K_{P,c} = 1 \tag{B.27}$$

As with the temperature in the previous section, the fractional exponent is $q=xr$, with $r=1/2$. As such, the fractional exponent for pressure is the same as that for temperature (i.e., $q=5/6$,). With the value of $K_{P,a}$ = 1.4125. Figure B.11 shows a plot of the circuit approximation for pressure based on Equation (B.26), compared to its scaled von Karman spectral of Equation (B.24).

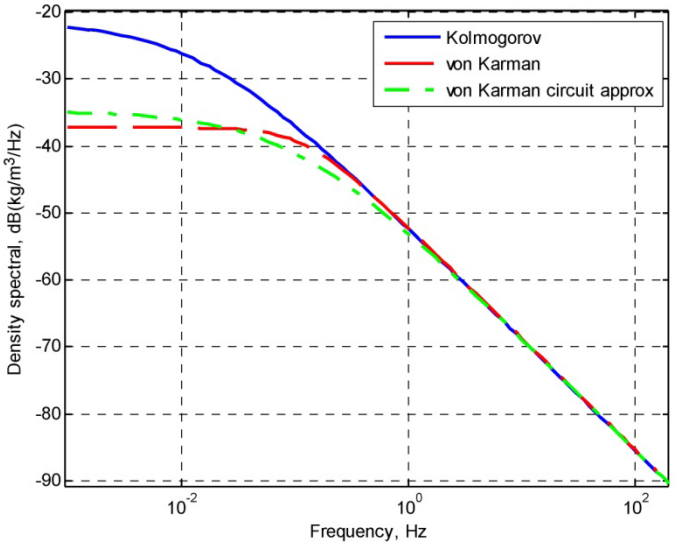

Figure B.12.—Kolmogorov and von Karman spectral for density and its von Karman circuit approximation (ε = 8.6e-5 m^2/sec^3, *L* = 762 m).

B.4 Density Disturbance

The density disturbance won't be needed when acoustic velocity, temperature and pressure disturbances are included in a simulation. However for completeness, density disturbance will be discussed here in brief. The magnitude of the density disturbance can be computed from the equation of state, $P=\rho RT$, by perturbing this equation, which can be solved as

$$\Delta\rho = \frac{P_o + \Delta P}{R(T_o + \Delta T)} - \frac{P_o}{RT_o} \tag{B.28}$$

where P_o and T_o are the standard atmospheric pressure and temperature in Pa and Kelvin respectively, which would be around 5500 Pa and 216 K at supersonic cruise. Figure B.12 shows a plot of the Kolmogorov, the Von Karman, and the circuit approximation spectral for density, all based on Equation (B.28) from values of temperature and pressure obtained in the previous sections. It can be seen from this figure that the Kolmogorov spectral obtained from Equation (B.28), actually looks like a finite von Karman spectral at low frequencies. Also, its low frequency asymptote would be approximately –20 dB, which equates to a density of 0.1 kg/m^3. From standard atmospheric tables, the atmospheric density at about 62,000 ft (i.e., at approximate cruise altitude) is also approximately 0.1 kg/m^3. Even though, at the limit as frequency approaches zero, the Kolmogorov spectral approximates the mean atmospheric density at cruise, the appropriate density disturbance would be that shown for the von Karman or the circuit approximation.

Appendix C.—Fractional Order TF Fits of Atmospheric Disturbances

Normally, with the derivation of circuit analogs and their respective TFs to describe atmospheric disturbances (as they were presented in the Appendix B), time domain simulations would be straightforward. However, these circuits and their TFs are fractional, which complicates performing time-domain simulations. The complication comes from a certain property of fractional order differential equations, which deals with non-locality. There are several works that deal with time domain solutions of fractional order differential equations Schmidt (2006) and Lorenzo (2008), but even to date, solving these types of differential equations is still challenging. Unlike integer order differential equations, the solution space of fractional order derivatives is not local and it depends on the whole prior history of the state, resulting in a state transition matrix that is in the form of a convolution integral. Therefore, solving the convolution at each time instant, taking into account all the prior history of the state, can be both complicated and taxing on the computing resources.

In this section the attempt will be to formulate an integer order approximation of the fractional order TF. Given the parameters describing an atmospheric disturbance, like eddy dissipation rate and integral length scale, the formulations will explicitly solve for the integer order TF poles and zeros that approximate the fractional order disturbance. This approach avoids the laborious process of hand fitting such an approximation, for every type of disturbance, and for every time an atmospheric disturbance parameter changes. After forming this approximation to the fractional order TF, and by selecting the frequencies of interest for the disturbance as an input to this TF approximation, the time domain atmospheric disturbance can be formed.

If the desire is to estimate the fractional order TF at each frequency decade by a single first order pole-zero pair, then the estimation process for each frequency decade starts with a pole followed by a zero (i.e., $\omega_{pi} < \omega_{zi}$), with one last pole placed after the last decade in order to keep attenuating the TF magnitude as

$$W_{t,o} \cong K\left(\prod_{i=1}^{n}\frac{s/\omega_{zi}+1}{s/\omega_{pi}+1}\right)\frac{1}{s/\omega_{pn+1}+1}W_t, \quad i=1,2,\ldots,n \qquad \text{(C.1)}$$

Where n is the number of pole-zero pairs of the estimated TF and K is the DC gain. So if the desire is to approximate the TF for three consecutive decades, with one pair of pole/zeros for each decade, starting at some desired frequency, then n would be three in this case. A sketch of this TF approximation as a staircase symmetrically located on top of the fractional order TF is shown in Figure C.1, with more description to follow later.

Thus, if one first order pole-zero pair is used to estimate each decade of the fractional order TF, the first pole should be placed at a certain frequency such that the pole gain dropping at a rate of –20 dB/decade, intersects the gain of the fractional order TF midway through, in the first decade. A fractional order TF gain would be decreasing at a rate q*20 dB/decade, where q is the fractional order. Therefore, midway through the first decade the initial gain is expected to decrease by a factor of *(½)*q*20 dB as

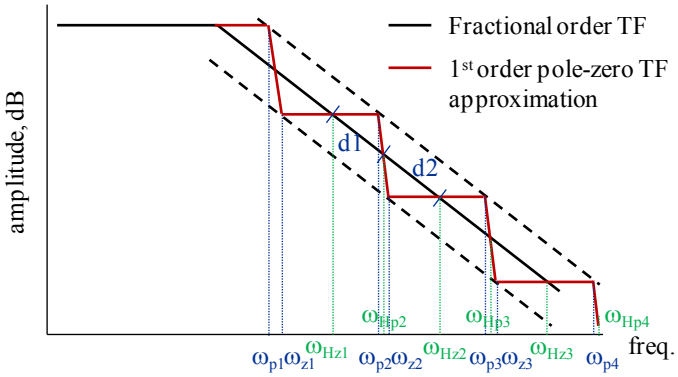

Figure C.1.—Pictorial diagram of fractional order TF fit.

$$\left.\frac{K}{s/\omega_{p1}+1}\right|_{s=1/2\text{decade}} = 10^{\frac{-1}{2}q(20)/20}K \qquad \text{(C.2)}$$

Divide by 20 is because of the $20\log_{10}(x)$ base scale. Solving for the frequency we get

$$\left.\omega_{p1}\right|_{s=1/2\text{decade}} = \frac{s}{10^{(1/2)q}-1} \qquad \text{(C.3)}$$

Also, midway in the first decade, the fractional TF, based on its circuit approximation in Appendix B, would have the same gain as that of Equation (C.2) as

$$\left.\frac{K}{(R_tC_ts)^q+1}\right|_{s=1/2\text{decade}} = 10^{\frac{-1}{2}q}K \qquad \text{(C.4)}$$

As was discussed in Appendix B, the natural frequency of the fractional order TF in Equation (C.4) is

$$\omega_n = \frac{1}{R_tC_t} \qquad \text{(C.5)}$$

Knowing ω_n, Equation (C.4) can be solved for s to find out at what frequency to place the first pole in order for the gains of these two TFs to intersect midway through the first decade as

$$\left.|s|\right|_{s=1/2\text{decade}} = \omega_n\left(10^{(1/2)q}-1\right)^{1/q} \qquad \text{(C.6)}$$

Substituting Equation (C.6) into Equation (C.3) for s, the frequency of the first pole can be solved as

$$\omega_{p1} = \omega_n \left(10^{(1/2)q} - 1\right)^{\frac{1-q}{q}} \tag{C.7}$$

So far in this development the assumption was that each decade of the fractional order TF will be approximated with one pole-zero pair as shown in Equation (C.1). Based on that, the estimated product of first order poles and zeros of Equation (C.1) will match the fractional order TF at half decade intervals. For that, the only distinction in Equation (C.7) is the 1/2 exponent in the right side of the equation. This successive ratio of desired decay matching, expressed here as H, can be generalized as

$$\omega_{p1} = \omega_n \left(10^{(H_{p1})q} - 1\right)^{\frac{1-q}{q}} \tag{C.8}$$

where H_{p1} is the decay ratio for the first pole, where the two TFs would match or the magnitudes will intercept.

Following the placement of the first pole, the need is to find out at what frequency to place the first zero of this pair. At the end of the first decade, the gain of the fractional TF would have dropped by $10^{-q}\,K$ as

$$\frac{K}{\left(R_t C_t s\right)^q + 1}\Big|_{s \text{ at first decade}} = 10^{-q} K \tag{C.9}$$

By substituting $1/\omega_f$, using Equation (C.5), for R_tC_t, the frequency s where the gain has dropped by the above magnitude can be calculated similarly as Equation (C.6)

$$|s|_{\text{at 1 decade}} = \omega_n \left(10^q - 1\right)^{1/q} \tag{C.10}$$

Or in general terms, as a function of the second portion of the approximation, $H_{z1,}$ desired to be matched (i.e., the first portion at ½ decade was matched with a pole, the second portion at 1 decade is matched with a zero (H_{z1}=1), and so on), this frequency can be expressed as

$$\omega_{Hz1} = \omega_n \left(10^{(H_{z1})q} - 1\right)^{1/q} \tag{C.11}$$

where

$$\omega_{Hz1} = |s|_{at H_{z1}(\text{decade})}$$

The purpose of the ω_H frequencies is to ensure symmetry (i.e., to symmetrically locate the TF approximation on top of the fractional order TF. Thus, in order to accomplish symmetry, the desire is to also have the estimating TF with the first pole-zero pair to equate to the same gain at this frequency, $\omega_{Hz1,}$ (i.e., the same gain as the right hand side of Equation (C.9), see also Figure C.1, as

$$\frac{K\left(s/\omega_{z1} + 1\right)}{s/\omega_{p1} + 1}\Big|_{s \text{ at 1 decade}} = 10^{-(H_{z1})q} K \tag{C.12}$$

From this equation, the frequency of the first zero can be calculated as

$$\omega_{z1} = \frac{\omega_{Hz1}}{10^{-(H_{z1})q}\left(\omega_{Hz1}/\omega_{p1} + 1\right) - 1} \tag{C.13}$$

Thus, choosing the ratio of decades at which it's desirable to match the TF estimate, Equations (C.2), (C.8), (C.11), and (C.13) can be used to compute the frequency of the first zero.

Following the same procedure to calculate the frequency of the second pole, by using Equation (C.9), but with the gain $10^{-(3/2)q}K$, (i.e., H_{p2}=1.5 decades),

$$\omega_{Hp2} = \omega_n \left(10^{(H_{p2})q} - 1\right)^{1/q} \tag{C.14}$$

Then using the TF with two poles and one zero equated to this gain, similar to Equation (C.12), the frequency of the second pole can be calculated as

$$\omega_{p2} = \frac{\omega_{Hp2}\left(\omega_{Hp2}/\omega_{p1} + 1\right)}{10^{(H_{p2})q}\left(\omega_{Hp2}/\omega_{z1} + 1\right) - 1} \tag{C.15}$$

The same procedure can be followed to calculate the rest of the frequencies of the poles and zeros of the estimating TF. In order to generalize these formulations (for approximating the fractional order TF), let's define ρ_{pz} as the desired density of pole-zero pairs per frequency decade. In addition, let's also define the number of equal decade subintervals (in log frequency scale) as η, where a pole or a zero will be used to closely match this TF as

$$\eta = \frac{1}{2\rho_{pz}} \tag{C.16}$$

Then, pole and zero vectors of decade intervals can be formed, where these TF will be closely matched as

$$H_p = \eta\,[2(1) - 1\;2(2) - 1 \ldots 2(m_p) - 1] \tag{C.17}$$

$$H_z = \eta[2(1)\;2(2) \ldots 2(m_z)] \tag{C.18}$$

For n number of decades over which to estimate the fractional order TF, m_p and m_z can be computed as

$$m_p = (n - 1)/\eta \tag{C.19}$$

$$m_z = m_p - 1 \tag{C.20}$$

For instance, for a density of one pair of pole-zeros per decade (i.e., ρ_{pz} =1) and estimating the TF for three decades (i.e., n=3), these vectors would have the values H_{pi} = [1/2 3/2 5/2 7/2], H_{zi} = [1 2 3].

Inspecting Equation (C.17), it can be seen that the first element of the vector, corresponding to the calculation of the first pole frequency, will always be equal to the value of η. Therefore, for convenience, Equation (C.8) can also be expressed in terms of η.

$$\omega_{p1} = \omega_n \left(10^{\eta q} - 1\right)^{\frac{1-q}{q}} \tag{C.21}$$

Also, inspection of the equations that describe the frequencies of the zeros and poles (i.e., Eqs. (C.11), (C.13), (C.14) and (C.15) respectively, it can be seen that a generalized relationship for these equations can be written as follows

$$\omega_{Hpi} = \omega_n \left(10^{(H_{pi})q} - 1\right)^{1/q} \tag{C.22}$$

A more generalized expression of Equation (C.22) can be arrived by substituting into it H_p from Equation (C.17) in terms of the pole number, i and η as

$$\omega_{Hpi} = \omega_n (10^{\eta(2i-1)q} - 1)^{1/q} \quad i = 2,\ldots,m_p \tag{C.23}$$

Then a generalized expression for the calculation of the pole placement frequencies can be formulated as

$$\begin{aligned}\omega_{pi} &= \\ &= \frac{K_{\omega pi}\omega_{Hpi}\left(\omega_{Hpi}/\omega_{pi-1}+1\right)\left(\omega_{Hpi}/\omega_{pi-2}+1\right)\ldots\left(\omega_{Hpi}/\omega_{pi1}+1\right)}{10^{(H_{pi})q}\left[\left(\omega_{Hpi}/\omega_{zi-1}+1\right)\left(\omega_{Hpi}/\omega_{zi-2}+1\right)\ldots\left(\omega_{Hpi}/\omega_{z1}+1\right)\right]-1} \\ &= \frac{K_{\omega pi}\omega_{Hpi}\prod_{j=1}^{i-1}\left(\omega_{Hpi}/\omega_{pi-j}+1\right)}{10^{\eta(2i-1)q}\prod_{j=1}^{i-1}\left(\omega_{Hpi}/\omega_{zi-j}+1\right)-1}, \quad i = 2,\ldots,m_p\end{aligned} \tag{C.24}$$

The proportionality factors $K_{\omega pi}$ have been inserted in case any final adjustments are needed to these frequencies to improve the TF fit.

Similarly, for the frequencies for placing the zeros

$$\omega_{Hzi} = \omega_n \left(10^{(H_{zi})q} - 1\right)^{1/q} \quad i = 1,2,\ldots,m_z \tag{C.25}$$

Or by substituting in Equation (C.21) the H_z vector from Equation (C.18) in terms of the zero number, i, and η as

$$\omega_{Hzi} = \omega_n \left(10^{2\eta iq} - 1\right)^{1/q} \quad i = 1,2,\ldots,m_z \tag{C.26}$$

Then a generalized expression for the calculation of the zero placement frequencies can be formulated as

$$\begin{aligned}\omega_{zi} &= \\ &= \frac{K_{\omega zi}\omega_{Hzi}\left(\omega_{Hzi}/\omega_{zi-1}+1\right)\left(\omega_{Hzi}/\omega_{zi-2}+1\right)\ldots\left(\omega_{Hzi}/\omega_{zi1}+1\right)}{10^{-(H_{zi})q}\left[\left(\omega_{Hzi}/\omega_{pi}+1\right)\left(\omega_{Hzi}/\omega_{pi-1}+1\right)\ldots\left(\omega_{Hzi}/\omega_{p1}+1\right)\right]-1} \\ &= \frac{K_{\omega zi}\omega_{Hzi}\prod_{j=1}^{i-1}\left(\omega_{Hzi}/\omega_{zi-j}+1\right)}{10^{-2\eta iq}\prod_{j=1}^{i}\left(\omega_{Hzi}/\omega_{pi}+1\right)-1} \quad \text{for } i = 1,2,\ldots m_z\end{aligned} \tag{C.27}$$

These formulations complete the computation of the pole-zero frequencies for the TF approximation of fractional order atmospheric disturbances. In terms of the indexes defined here, Equation (C.1) can be rewritten as

$$W_{t,o} \cong K_{t,fit}\frac{\prod_{1}^{m_z}\left(s/\omega_{zi}+1\right)}{\prod_{1}^{m_p}\left(s/\omega_{pi}+1\right)}W_t \tag{C.28}$$

As described in Appendix B, the von Karman spectral, Equations (B.2) and (B.3), can be approximated with a fractional order circuit with a natural frequency that can be determined using Equation (B.8). Equation (B.8) is conveniently reproduced below in Equation (C.29).

$$\omega_n = \frac{K_{\omega n}}{R_t C_t} \tag{C.29}$$

with an equivalent capacitance and resistance for the type of disturbance t, derived as Equation (B.13) and (B.14)

$$C_t = \frac{1}{\left(a_t \varepsilon^{2/3}\right)^{1/x}\left(2\pi M a\right)} \tag{C.30}$$

$$R_t = 1.339\left(2\pi\right)\left(a_t \varepsilon^{2/3}\right)^{1/x} L \tag{C.31}$$

Based on these derivations, TF approximations of fractional order atmospheric turbulences can be developed (for the von Karman spectral, for any fractional order $0 < q < 1$) by using Equation (C.28), together with supporting Equations (C.16), (C.19) to (C.21), (C.25) to (C.27), (C.23) to (C.24) and (C.26) to (C.27), (C.29) to (C.31).

In a pictorial sense, by referring back to Figure C.1, the first order pole-zero pair TF approximation of a fractional order atmospheric turbulence can be viewed as a staircase symmetrically located on top of the fractional order TF. The utility of ω_{Hpi} and ω_{Hzi} are to maintain this symmetry. This is accomplished in the derivations above by formulating the symmetry frequencies, ω_H's, such that the length segments between intercepts (like $d1$ and $d2$) or alternatively the horizontal distances on either side of the intercepts are equal.

In the subsections that follow, more detail will be discussed about developing the approximations for each type of

disturbance. In addition, some final adjustments that need to be made to the pole-zero frequencies and the proportionality constants K will be presented. Without these final adjustments, the fits will resemble the example fit shown in Figure C.2, with the fractional order fit winding its way around the fractional order TF

C.1 Longitudinal and Transverse Acoustic Wave Disturbances—TF Fits

By applying the formulations derived in Section C.1, TF fits for the longitudinal and transverse atmospheric disturbances can be constructed based on Equation (C.28). Figure C.3 shows a plot of the longitudinal von Karman disturbance of Equation (B.2), it's circuit TF approximation reproduced from Figure B.2, and the TF fit computed using the equations derived previously in this Appendix for $q=xr=5/9$ (i.e., $x=5/3$, $r=1/3$), $\eta=1/2$, $n=3$ (decades), and with atmospheric turbulence parameters ε=8.6e-5 (m^2/sec^3) and L=762 m.

The maximum error in this TF fit for the circuit approximation, using 4 poles and 3 zeros, over a span of 3½ decades, amounts to approximately 1.5 dB. The error for the actual von Karman spectral is larger; about 4 dB at 0.1 Hz and decreases as the frequency increases. Assuming, that the control system design can sufficiently attenuate frequencies at this low frequency range (as it should) then this TF fit approximation can be acceptable for the actual von Karman spectral. For the TF fit shown in Figure C.3, which is an approximation to the longitudinal von Karman spectral of Equation (B.2) the pole and zero frequencies in Equation (C.28) are

$$\begin{aligned} \omega_{pi} &= [0.6 \;\; 12.54 \;\; 85.71 \;\; 2062.0], \\ \omega_{zi} &= [3.82 \;\; 22.92 \;\; 312.38] \end{aligned} \quad \text{(rad/sec)} \qquad \text{(C.32)}$$

with $K_{l,\text{fit}}$ in Equation (C.28) given by the numerator in Equation (5) raised to 1/3 power to account for the units conversion as

$$K_{l,\text{fit}} = \left(5.4\varepsilon^{2/3}L^{5/3}\right)^{\frac{1}{3}} \qquad \text{(C.33)}$$

The preceding development to derive the equations to approximate a fractional order TF was based on a single fractional order TF, and a circuit approximation to the atmospheric disturbance was used for this development. However, as indicated by Equation (B.2) and (B.3), the von Karman spectral is not that of a single order fractional TF, especially in the lower frequency spectral. Therefore, for better accuracy, the derived equations can be adjusted to better fit the von Karman spectral. Examining Figure C.3, it can be seen that the TF fit can better approximate the von Karman

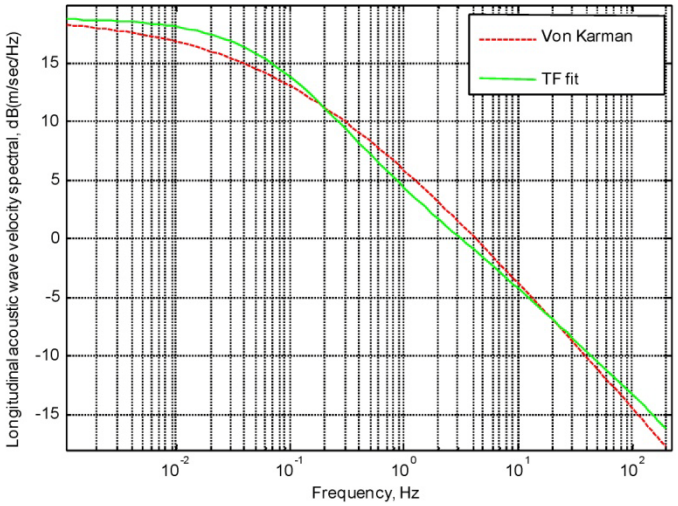

Figure C.2.—An example Fit without final adjustments to proportionality factors and frequencies.

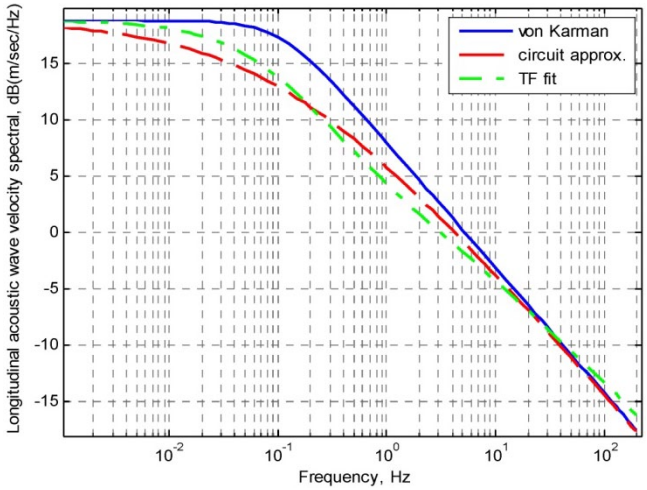

Figure C.3.—Longitudinal von Karman spectral, circuit approximation, and TF fit (ε = 8.6e-5 m^2/sec^3, L = 762 m).

spectral if the natural frequency ω_n, Equation (C.5), is increased, about proportionally to the difference in magnitudes between the fractional order TF and the approximation TF, at that frequency. However, doing that will also increase the pole-zero frequencies of the TF fit based on the equations derived. Therefore, some equivalent adjustment to some of these frequencies will need to be made. Figures C.4 and C.5 show the TF fit for the longitudinal and transverse von Karman disturbances respectively, with the following adjustments to Equations (C.24), (C.29) and (C.27)

$$K_{l/v,\omega} = \left[K_{\omega n}; K_{\omega pi}; K_{\omega zi}\right] = \left[2.4;\ 1\ \ 1\ \ 1/2.4\ \ 1/1.5;\ \ 1\ \ 1\ \ 1\right] \tag{C.34}$$

With $K_{l/v,\omega}$ symbolizing the proportionality constants for the frequency adjustments for both the longitudinal and transverse disturbances, which gives the frequency values of (for ε=8.6e-5 m^2/sec^3 and L=762 m)

$$\omega_{pi} = \left[1.46\ \ 30.10\ \ 85.71\ \ 1593.1\right], \quad \omega_{zi} = \left[9.18\ \ 55.02\ \ 335.48\right] \tag{C.35}$$

The proportionality factor, $K_{l,\text{fit}}$, in Equation (C.28) is given again by Equation (C.33). Similarly, $K_{v,\text{fit}}$ is developed using Equation (B.6) as follows, but also adjusting by 3 dB which will appropriately raise its magnitude in order to match the high frequency asymptote as

$$K_{v,fit} = 1.4\left(2.7\varepsilon^{2/3}L^{5/3}\right)^{\frac{1}{3}} \tag{C.36}$$

As can be seen in Figure C.5, the TF fit of the transverse disturbance is not very accurate at the low frequency, which would normally be fine for control system design purposes as discussed before. But it may not be acceptable, for let's say, wing loading. Thus, further adjustments could be made if desirable. For instance, instead of multiplying $K_{v,\text{fit}}$ with the 3 dB gain of 1.4, the natural frequency ω_n of Equation (C.29) could be multiplied by this factor to raise its frequency. Then for final adjustments, the natural frequency can be also multiplied by the ratio of the difference of frequencies between the fit and the actual von Karman spectral obtained at some fixed amplitude, at some high frequency. This can be done either graphically or analytically. Performing these manipulations, a better fit of the transverse disturbance is shown in Figure C.6, with a final value of $K_{\omega n}$ = 4.27. This will result in the following adjustments for the transverse disturbance

$$K_{v,\omega} = \left[K_{\omega n}; K_{\omega pi}; K_{\omega zi}\right] = \left[4.27;\ 1\ \ 1\ \ 1/2.4\ \ 1/1.5;\ \ 1\ \ 1\ \ 1\right] \tag{C.37}$$

which gives the frequency values of (for ε=8.6e-5 m^2/sec^3 and L=762 m)

$$\omega_{v,pi} = \left[2.60\ \ 53.56\ \ 152.55\ \ 2835.3\right], \quad \omega_{v,zi} = \left[16.33\ \ 97.92\ \ 597.07\right] \tag{C.38}$$

with a $K_{v,\text{fit}}$ expression as

$$K_{v,\text{fit}} = \left(2.7\varepsilon^{2/3}L^{5/3}\right)^{\frac{1}{3}} \tag{C.39}$$

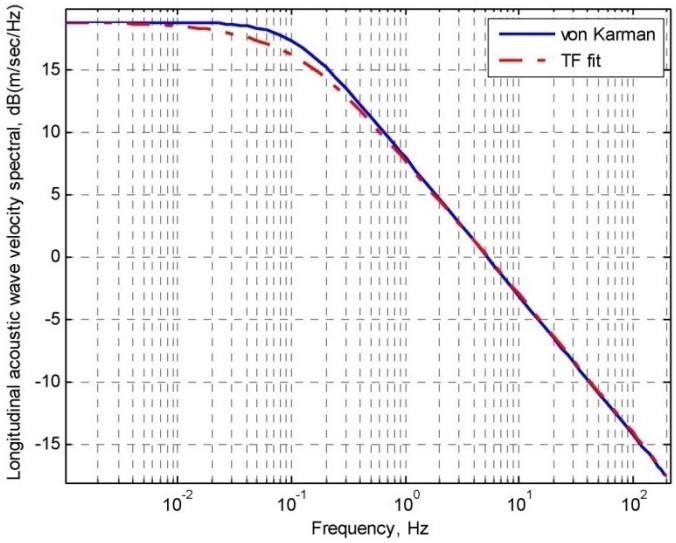

Figure C.4.—Longitudinal von Karman spectral, adjusted TF fit (ε = 8.6e-5 m^2/sec^3, L = 762 m).

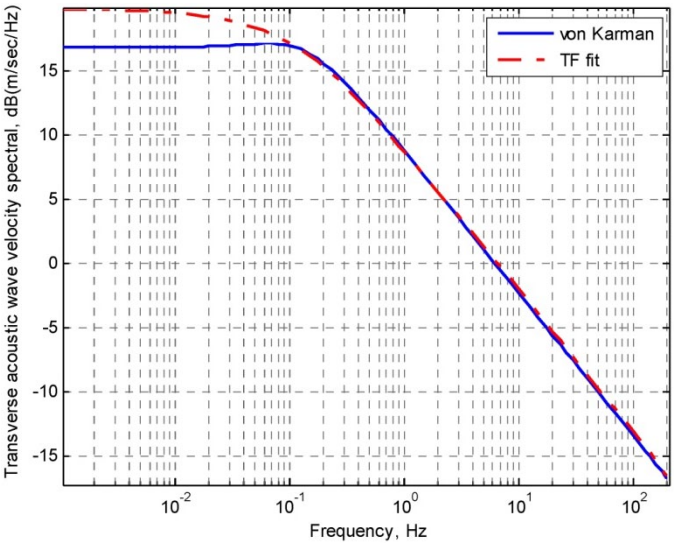

Figure C.5.—Transverse von Karman spectral, adjusted TF fit (ε = 8.6e-5 m^2/sec^3, L = 762 m).

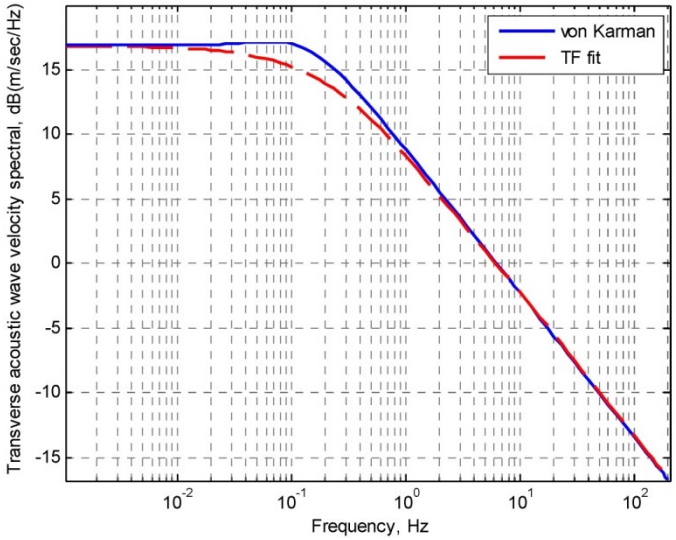

Figure C.6.—Transverse von Karman spectral, final adjusted TF fit (ε = 8.6e-5 m^2/sec^3, L = 762 m).

C.2 Temperature Disturbance—TF Fit

As discussed before, the units conversion factor for temperature is r=1/2, which makes the fractional exponent value q=5/6 (x=5/3). Substituting this value for the fractional exponent, with the same values of η, n, and with the same atmospheric parameter values as those used for the longitudinal and transverse acoustic disturbances, and again using the formulations previously developed in this Appendix, the poles and zeros for the TF fit can be directly computed as before. The resulting TF fit with $K_{t,\text{fit}}$ in Equation (C.28) given by Equation (B.20) raised to the ½ power as

$$K_T = \left(14.0\varepsilon^{2/3}L^{5/3}\right)^{\frac{1}{2}} \tag{C.40}$$

This fit (not shown here) will end-up with the same low and high frequency asymptotes as with the von Karman form, but at somewhat lower frequency. Similarly to the longitudinal disturbance, this can be corrected by multiplying $K_{\omega n}$ in Equation (C.29) by 3/2, which turns out to be the ratio of the frequencies of these two spectra at some high frequency, for select fixed amplitude. Finally, by some minor adjustments to the high frequency poles, these spectra can be matched fairly close, as shown in Figure C.7. This will result in the following adjustments for the temperature disturbance

$$\begin{aligned} K_{T,\omega} &= \left[K_{\omega n}; K_{\omega pi}; K_{\omega zi}\right] \\ &= \left[1.5;\ 1\ \ 1\ \ 1/1.1\ \ 1/1.2;\ 1\ \ 1\ \ 1\right] \end{aligned} \tag{C.41}$$

which gives the frequency values of (for ε=8.6e-5 m^2/sec^3 and L=762 m)

$$\begin{aligned} \omega_{T,pi} &= \left[1.10\ \ 25.11\ \ 109.77\ \ 816.35\right], \\ \omega_{T,zi} &= \left[33.04\ \ 45.64\ \ 602.36\right] \end{aligned} \tag{C.42}$$

with a $K_{T,\text{fit}}$, using Equation (B.20) as

$$K_{T,\text{fit(temp)}} = \left(14.0\varepsilon^{2/3}L^{5/3}\right)^{1/2} \tag{C.43}$$

If the desire is to simulate the acoustic disturbance generated by a temperature gust, this conversion can be done by utilizing the perturbation relation of the speed of sound with temperature described in Appendix B (Eq. (B.23)) as

$$\Delta v = \frac{M\gamma R}{2a_o}\Delta T \tag{C.44}$$

Together with Equation (C.36) to adjust $K_{T,\text{fit}}$ as

$$K_{T,\text{fit(acoustic)}} = \frac{M\gamma R}{2a_o}\sqrt{14.0\varepsilon^{2/3}L^{5/3}} \tag{C.45}$$

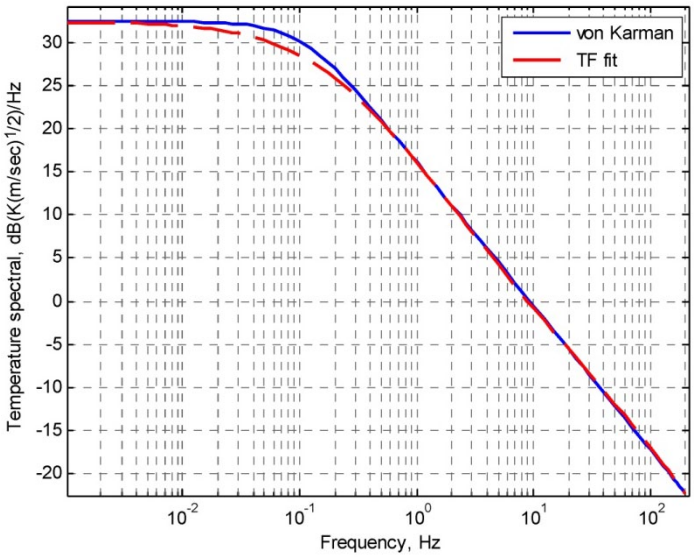

Figure C.7.—Temperature von Karman spectral and its TF fit (ε=8.6e-5 m^2/sec^3, L=762 m).

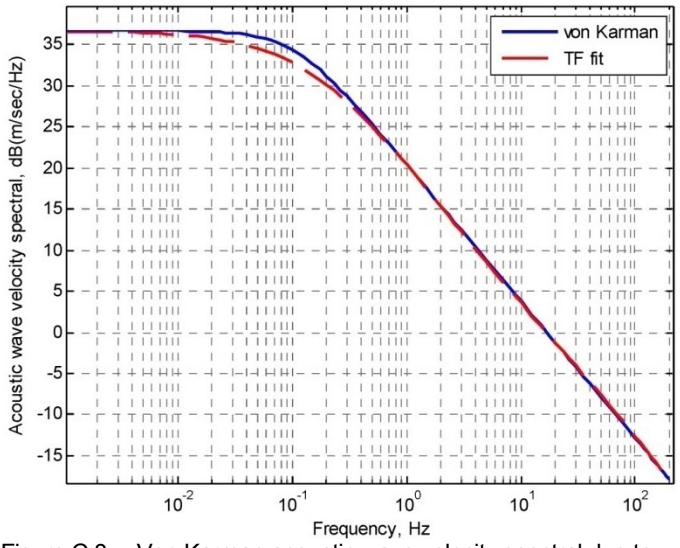

Figure C.8.—Von Karman acoustic wave velocity spectral due to temperature gust and its TF fit (ε = 8.6e-5 m^2/sec^3, L = 762 m).

The acoustic velocity disturbance due to a temperature gust, at approximate supersonic cruise altitude is shown in Figure C.8.

Based on all the derivations carried out so far, the TF fits should work for different values of atmospheric parameters (like those of Eq. (C.45)). Figures C.9 and C.10 as compared to Figures 3 and 4 for their shape, show the TF fits with different values of eddy dissipation rates and integral scale lengths, by employing the same TF fit equations and without changing any other parameters, like the $K_{T,\omega}$ values, Equation (C.41).

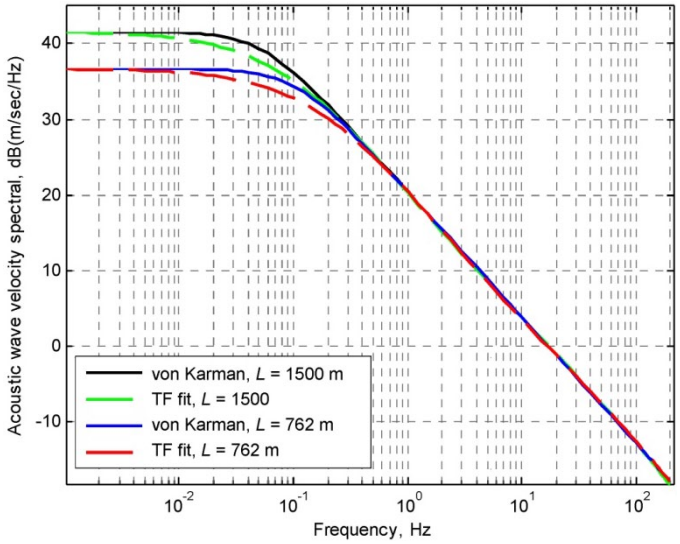

Figure C.9.—Von Karman acoustic wave velocity spectral due to temperature gust and its TF fits for different integral scale lengths (ε = 8.6e-5 m^2/sec^3).

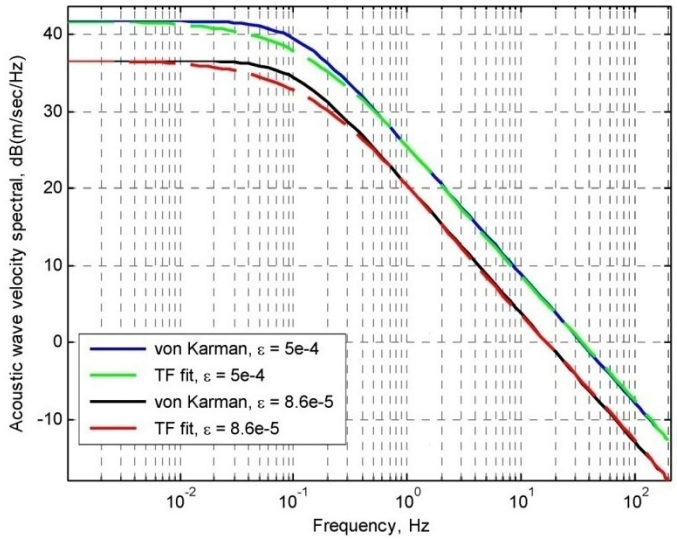

Figure C.10.—Von Karman acoustic wave velocity spectral due to temperature gust and its TF fits for different eddy dissipation rates (*L*=762 m).

C.3 Pressure Disturbance—TF Fit

The units conversion factor for pressure is the same as that for temperature (i.e., r=1/2), which also makes the fractional exponent value q=5/6. Substituting this value for the fractional exponent, with the same values of η, n, and H as those used for the longitudinal, transverse and temperature disturbances, and again using Equations (C.16), (C.19) to (C.21), (C.25) to (C.27), (C.23) to (C.24) and (C.26) to (C.27), (C.29) to (C.31), the poles and zeros for the TF fit for pressure can be computed as before. The resulting TF fit, with $K_{t,\text{fit}}$ in Equation (C.28) given by Equation (B.25) raised to the ½ power, is shown in Figure C.11. It turns out, that adjustments to $K_{P,\omega}$ are exactly the same as those for $K_{T,\omega}$, Equation (C.41). For completeness, these frequency adjustments and the $K_{P,\text{fit}}$ equation for pressure disturbances are listed below.

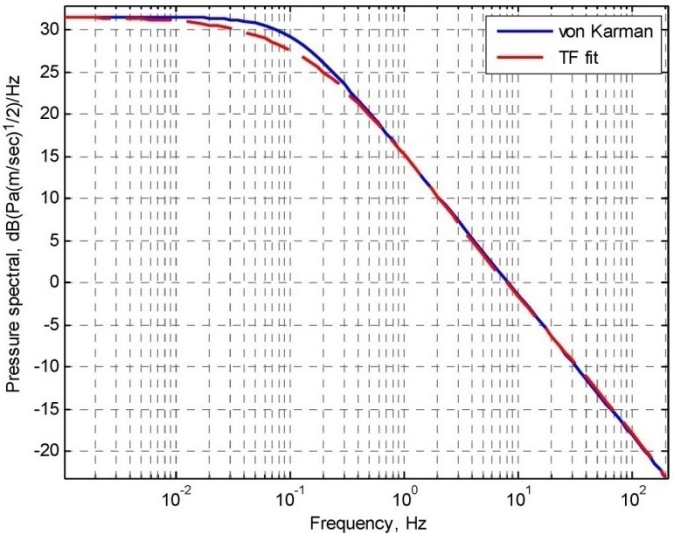

Figure C.11.—Pressure von Karman spectral and its TF fit (ε = 8.6e-5 m^2/sec^3, *L* = 762 m).

$$K_{P,\omega} = \left[K_{\omega n}; K_{\omega pi}; K_{\omega zi}\right] = \left[1.5;\ 1\ \ 1\ \ 1/1.1\ \ 1/1.2;\ \ 1\ \ 1\ \ 1\right] \tag{C.46}$$

which gives the frequency values of (for ε=8.6e-5 m^2/sec^3 and L=762 m)

$$\omega_{P,pi} = \left[1.10\ \ \ 25.11\ \ \ 109.77\ \ \ 816.35\right], \quad \omega_{P,zi} = \left[33.04\ \ \ 45.64\ \ \ 602.36\right] \tag{C.47}$$

with a $K_{P,\text{fit}}$, using Equation (B.25) as

$$K_{P,\text{fit}} = \sqrt{11.6\varepsilon^{2/3}L^{5/3}} \tag{C.48}$$

C.4 Density Disturbance—TF Fit

As discussed in Section B.4, once the temperature and pressure TF fits have been calculated based on the formulations in the previous two sections, the density disturbance can be directly obtained by utilizing Equation (B.28). A plot of this density spectral is shown in Figure C.12.

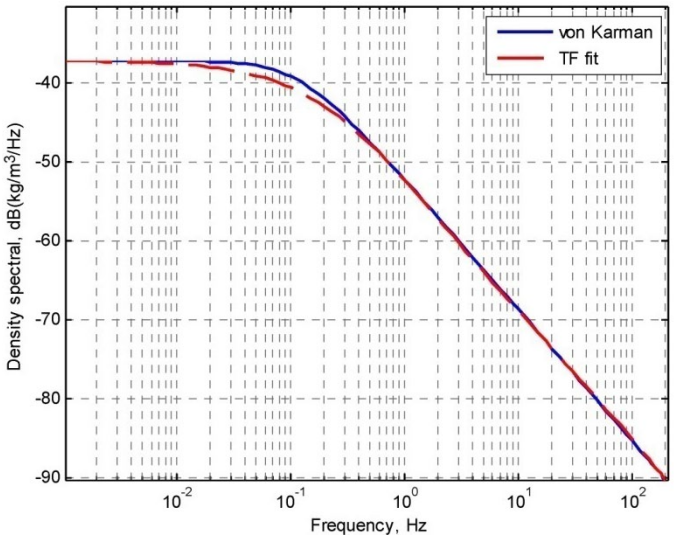

Figure C.12.—Density von Karman spectral and its TF fit (ε = 8.6e-5 m^2/sec^3, L = 762 m).

References

Anderson, J.D., Jr., (2000): "Introduction to Flight," Fourth Edition, McGraw-Hill Series in Aeronautics and Aerospace Engineering.

Ashun, U., (2004): "Dynamic Characterization and Active Control of Unstarts in a Near-Isentropic Supersonic Inlet," Master's Thesis, Massachusetts Institute of Technology, Feb. 2004.

Fairall, C.W., White, A.B. and Thompson, D.W., (1991): "A Stochastic Model of Gravity-Wave-Induced Clear-Air Turbulence," Journal of Atmospheric Sciences, Vol. 48, No. 15, Aug. 1991.

Hoblit, F.M., (1988): "Gust Loads on Aircraft: Concepts and Applications," America Institute of Aeronautics & Astronautics, AIAA Education Series.

Houbolt, J.C., Steiner, R., and Pratt, K.G., (1964): "Dynamic Response of Airplanes to Atmospheric Turbulence Including Flight Data on Input Response," NASA TR R–199, Jun. 1964.

Kolmogorov, A.N., (1941(a)): "Dissipation of Energy in the Locally Isotropic Turbulence," Comptes rendus (Doklady) de l'Académie des Sciences de l'U.R.S.S., 32, 16–18, 1941.

Kolmogorov, A.N., (1941(b)): "The Local Structure of Turbulence in Incompressible Viscous Fluid for Very Large Reynolds' Numbers," Comptes rendus (Doklady) de l'Académie des Sciences de l'U.R.S.S., 30, 301–305.

Kopasakis, G., (2010): "Modeling of Atmospheric Turbulence as Disturbance for Control Design and Evaluation of High Speed Propulsion Systems," GT2010–22851, ASME TurboExpo, Jun. 2010.

Lorenzo, C.F. and Hartley, T.T. (2008): "Initialization of Fractional-Order Operators and Fractional Differential Equations," ASME Journal of Computational and Nonlinear Dynamics, Vol. 3, Issue 2, Apr. 2008.

McMinn, J.D., (1997): "Extension of a Kolmogorov Atmospheric Turbulence Model for Time-Based Simulation Implementation," AIAA Guidance, Navigation and Control Conference, New Orleans, LA, Aug. 11–13, 1997, AIAA–97–3532.

Nastrom, G.D. and Gage, K.S. (1985): "A Climatology of Atmospheric Wavenumber Spectra of Wind and Temperature Observed by Commercial Aircraft," Journal of Atmospheric Sciences, Vol. 42, No. 9, May 1985, pp. 950–960.

Obukhov, A. M., (1949): "Structure of the Temperature Field in Turbulent Flow," Translation Izvestiin Akademii, Nauk S.S.S.R., Ser. Geogr. i Geofiz., Vol. 13, No. 1, pp. 58–69.

Schmidt, A. and Lothar, G., (2006): "On the numerical Evaluation of Fractional Derivatives in Multi-Degree-of-Freedom Systems," Elsevier North-Holland, Inc., Fractional Calculus Applications in Signals and Systems, Vol. 86, Issue 10, pp. 2592–2601, Oct. 2006.

Soreide, D.C. and Tank, W.G., (1996): "Proposed Model of the Atmosphere for the High Speed Civil Transport Program," Program Report, March 1996.

Soreide, D.C. and Tank, W.G., (1997): "Validation of a statistical Atmospheric Model Using 747 Vertical Gust Exceedance Data," AIAA–975579.

Tank, W.G. (1994): "Atmospheric Disturbance Environmental Definition," NASA CR–195315, Feb. 1994.

Tank, W.G. and Gillis, J., (1996): "Atmospheric Disturbance Models for Linear and Nonlinear System Response Analysis," AIAA 34th Aerospace Sciences Meeting and Exhibit, Reno, NV, AIAA–1996–394, Jan. 1996.

Tatarski, V.I., (1961): "Wave Propagation in a Turbulent Medium," McGraw-Hill.

REPORT DOCUMENTATION PAGE	Form Approved OMB No. 0704-0188

1. REPORT DATE *(DD-MM-YYYY)*	2. REPORT TYPE	3. DATES COVERED *(From - To)*
01-12-2010	Technical Memorandum	

4. TITLE AND SUBTITLE
Atmospheric Turbulence Modeling for Aero Vehicles: Fractional Order Fits

5a. CONTRACT NUMBER

5b. GRANT NUMBER

5c. PROGRAM ELEMENT NUMBER

6. AUTHOR(S)
Kopasakis, George

5d. PROJECT NUMBER

5e. TASK NUMBER

5f. WORK UNIT NUMBER
WBS 984754.02.07.03.20.02

7. PERFORMING ORGANIZATION NAME(S) AND ADDRESS(ES)
National Aeronautics and Space Administration
John H. Glenn Research Center at Lewis Field
Cleveland, Ohio 44135-3191

8. PERFORMING ORGANIZATION REPORT NUMBER
E-17566

9. SPONSORING/MONITORING AGENCY NAME(S) AND ADDRESS(ES)
National Aeronautics and Space Administration
Washington, DC 20546-0001

10. SPONSORING/MONITOR'S ACRONYM(S)
NASA

11. SPONSORING/MONITORING REPORT NUMBER
NASA/TM-2010-216961

12. DISTRIBUTION/AVAILABILITY STATEMENT
Unclassified-Unlimited
Subject Categories: 01, 02, 03, 05, 07, 08 and 15
Available electronically at http://gltrs.grc.nasa.gov
This publication is available from the NASA Center for AeroSpace Information, 443-757-5802

13. SUPPLEMENTARY NOTES

14. ABSTRACT
Atmospheric turbulence models are necessary for the design of both inlet/engine and flight controls, as well as for studying coupling between the propulsion and the vehicle structural dynamics for supersonic vehicles. Models based on the Kolmogorov spectrum have been previously utilized to model atmospheric turbulence. In this paper, a more accurate model is developed in its representative fractional order form, typical of atmospheric disturbances. This is accomplished by first scaling the Kolmogorov spectral to convert them into finite energy von Karman forms and then by deriving an explicit fractional circuit-filter type analog for this model. This circuit model is utilized to develop a generalized formulation in frequency domain to approximate the fractional order with the products of first order transfer functions, which enables accurate time domain simulations. The objective of this work is as follows. Given the parameters describing the conditions of atmospheric disturbances, and utilizing the derived formulations, directly compute the transfer function poles and zeros describing these disturbances for acoustic velocity, temperature, pressure, and density. Time domain simulations of representative atmospheric turbulence can then be developed by utilizing these computed transfer functions together with the disturbance frequencies of interest.

15. SUBJECT TERMS
Atmospheric turbulence; Atmospheric disturbances; Flight controls; Propulsion controls; Flight loads; Propulsion disturbances; Aeroservoelastic disturbances; AeroPropulsoServoElasticity; Gust loads; Vehicle gust loads

16. SECURITY CLASSIFICATION OF:			17. LIMITATION OF ABSTRACT	18. NUMBER OF PAGES	19a. NAME OF RESPONSIBLE PERSON
a. REPORT	b. ABSTRACT	c. THIS PAGE			STI Help Desk (email:help@sti.nasa.gov)
U	U	U	UU	32	19b. TELEPHONE NUMBER *(include area code)* 443-757-5802